Recent Progress in the Preparation, Properties and Applications of Superhydrophobic Nano-based Coatings and Surfaces : A review

Phuong Nguyen-Tri[1*], Hai Nguyen Tran[2], Claudiane Ouellet Plamondon[3], Dai-Viet N. Vo[4], Sonil Nanda[5], Abhilasha Mishra[6], Huan-Ping Chao[7,8], A.K. Bajpai[9]

[1]Department of Chemistry, University of Montreal, Quebec, Canada

[2]Institute of Research and Development, Duy Tan University, Da Nang 550000, Vietnam

[3]Department of Civil Engineering, École de Technologie Supérieure, Montreal, QC, Canada

[4]Faculty of Chemical & Natural Resources Engineering, Universiti Malaysia Pahang, Gambang, Malaysia

[5]Department of Chemical and Biochemical Engineering, University of Western Ontario, Ontario, Canada

[6]Chemistry Department, Graphic Era University, Dehradun, India

[7]Department of Environmental Engineering, Chung Yuan Christian University, Chungli 320, Taiwan.

[8]R&D Center for Membrane Technology, Chung Yuan Christian University, Chungli 320, Taiwan.

[9]Bose Memorial Research Laboratory, Department of Chemistry, Government Autonomous Science College, Madhya Pradesh, India

*Corresponding author (P. Nguyen-Tri):

Email: Phuong.nguyen.tri@umontreal.ca, Tel: + 514-340 5121 (7326)

Authors' accepted manuscript
Article published in *Progress in Organic Coatings*, Vol. 132 (July 2019), Pages 235-256
https://doi.org/10.1016/j.porgcoat.2019.03.042

Table of Contents

Abstract

With the recent progress in nanotechnology and material engineering, nano-based coatings have become multifunctional, smarter, efficient, versatile and durable. Superhydrophobic coatings are an important class of the smart coating family, which has gained recognition in coating science over the last few years. The uniqueness of superhydrophobic coatings arises from the various phenomenal innovations, and its development is expected to continue in the next decades. . The bioinspired superhydrophobic surfaces are commonly obtained by designing a double-scale structure by using nanotechnology, followed byis the addition of water repellent compounds. It lacks an overview article describing the recent progress in superhydrophobic coatings and surfaces. In this perspective article, various fundamental aspects of wettability and related phenomena are discussed. We then present and compare the existing methods for superhydrophobic coating preparation. Superhydrophobic properties of superhydrophobic coatings such as self-cleaning, anti-icing, anti-fouling, and anti-bacterial features were then introduced. The review also discusses various superhydrophobic technological breakthroughs and future trends in the preparation and application of these materials.

Keywords: Superhydrophobic coating; interfaces; nanoparticles; water repellent; perfluorinated compounds; silane.

1. Introduction

Nanostructures materials have gained wide attention in the recent times owing to their unique characteristics as opposed to the precursor bulk material (add new references). Today, the nano-based coatings not only serve as protection layers against mechanical aggressors or decorative purposes, but also act as smart materials that are multifunctional. According to the literature, smart coatings can be applied for anti-corrosion,[1, 2] anti-wearing,[3] anti-bacterial,[4-7] anti-fungal,[8, 9] self-cleaning,[10, 11] superhydrophobic,[12, 13] solar reflective,[14, 15] photocatalytic,[16-19] and radar absorbing[20] and electrically conducting polymeric[21] applications. For example, lotus leaf [22] with naturally attained superhydrophobic and self-cleaning effects has garnered great interest among the researchers due to its potential biomimicking in coatings for self-cleaning,[23] anti-icing,[12, 24] anti-fog,[12, 25, 26] anti-wetting,[27] and anti-fouling.[28, 29] Superhydrophobic surfaces with self-cleaning properties are caused by rough structures with double scales of texture. These are characterized by a surface roughness of microstructures and nanostructures, (double hierarchical structures) covered by an organic wax.

Superhydrophobic and superoleophobic coatings are an important class of smart coatings creating great interest among researchers worldwide. More than eleven thousands articles related to superhydrophobic materials are being published in the Information Sciences Institute (ISI) indexed journals each year.[30] The number of publications in this field is expected to dramatically increase in the forthcoming years. Although there are some review papers on similar topics, they lack a systematic overview of various superhydrophobic coatings (SHCs) and surfaces from the fundamentals to the applications of interest. This review emphasizes on the recent developments in the preparation, properties, characterization and applications of superhydrophobic coatings and surfaces that can be applied in various fields including informed opinions of the authors on these topics. Several fundamental aspects on wettability and related phenomena are also reported and discussed. Moreover,

the attributes of superhydrophobic materials—self-cleaning, anti-biofouling, anti-bacterial, anti-icing, anti-fogging, anti-corrosion, and water/oil repellent—have been discussed vividly for relevant real-world applications.

2. Superhydrophobic surfaces in nature

In nature, superhydrophobic surfaces are found in some plants, insect species and animal kingdoms with water active properties and mimesis to allow them to better survive in their environment.[31-34] The main purposes of natural superhydrophobic layers are to prevent water accumulation, have a low adhesion to extraneous substances, facilitate droplet rolling to encapsulate contaminants at their surface, and sometimes to discourage microbial growth. The superhydrophobic layer on the surface of mosquitoes' eyes serves for anti-fogging. The self-cleaning properties in plants is to remove the solid and liquid contaminants that can interfere with photosynthesis.[35] The cuticle of the planthopper insect wing has anti-bacterial properties.[35] In all these natural scenarios, the low contact angle hysteresis (CAH) contributes to the self-cleaning properties and the reduction of drag in fluid flow.[36]

The superhydrophobic property has a combination of functions possible by the material structure. The geometrical arrangement of nanostructures interact with the light, which generates optical properties for harvesting and protection, communication, sensing, camouflage, mimesis, and mate attraction.[37] The annual legume *Melilotus siculus* has a gas layer that physically separates the seawater from the leaves, which allows the plant to survive in saline water and achieve photosynthesis under complete submergence.[31] The nanopillars in butterfly and cicada wings enhance the surface roughness and anti-wetting properties, which results in self-cleaning and anti-fouling.[37] These attributes also possess photonic features with iridescent and anti-reflection function.

The superhydrophobic properties in nature arise from the structural arrangement of simple building blocks,[31] rather than the chemical diversity.[37] The superhydrophobic design forms four general groups such as: (i) simple like pillars and dome shape, (ii) varied shape of a few micrometers in one dimension, (iii) hair or setae usually longer than 5 μm with a much smaller diameter, and (iv) hierarchical organization that is a combination of these elements.[34] The hierarchical micro- and nanostructures combined with low surface energy create the superhydrophobic surface.[33, 38] For example, the lotus leaf was annealed to destroy the nanoscale features, whereas the water contact angle was recorded to be reduced.[39] Thus, the high contact angle is the result of the microscale surface roughness and nanoscale hair-like structures. Indeed, the lotus leaf has thousands of micro-papillae on its surface,[40-42] which provides the first natural protective layer. In addition, the micro-papillae are covered with a second rough surface at the nanoscale. The shape and density of the papillae allow the lotus leaves to have a weak contact zone between the leaf surface and the water droplet.

The structure in insects maximize the air-water interface area and minimize the solid-water area.[34] The structure of the natural superhydrophobic coatings also trap air in their surface,[38] which induces the negative Laplace pressure difference at the liquid-vapor interface preventing the liquid to enter the surface.[31] Superhydrophobic coatings in nature are well explained by the increase in roughness from the Wenzel effect and the Cassie-Baxter principles of heterogeneous composition of air and solid where the trapped air enhances the non-wetting properties.[34, 36] The hierarchical structure enhances the static contact angle and reduces the contact angle hysteresis, which is the difference between the advancing and receding contact angles. [36]

Various plant kingdoms containing superhydrophobic layer with double hierarchical textures are found in nature. The lotus leaf (*Nelumbo nucifera*) has papillose epidermal cells covered with epicuticular wax tubules,[31, 33] which minimize the contact area of liquid and dirt on the surface.[38] The

texture on taro leaves (*Colocasia esculenta*) has 10 µm elliptic protrusions uniformly distributed on the surface, as well as nano-textured pins disseminated on the surface. The rice leaves (*Oryza sativa* L.) contain papillae ordered parallel to the edge of 5–8 µm in diameter resulting in anisotropic texture that allows water droplets to roll off in the direction of the edges.[38] Sub-nanometer pins on the sublayer are distributed on the paddy leaf surface to increase the air trapped. The water fern *(Salvinia molesta*) has multicellular hairs containing a microscopic egg-beater structure with hydrophobic patches. The contact angle, epidermal relief and epicuticular wax crystals of over 200 species of water-repellent and self-cleaning plant surface is reported.[43] Their epidermises are qualified in botanical terms as convex, papillose, hairy, or smooth. The epicuticular wax crystals are tubules, platelets, ribbons, coiled rodlets, rodlets, dendritic, threads, and cuticular folds.

The superhydrophobic behaviour in insects also features regular repeated patterns of double architectural texture. The planthopper (*Desudaba danae*) insect wing has an architectural arrangement analogue to the lotus leaves.[35] This insect is found in the same environment with lotus plants, thus exposed to the similar frequency of rainfall and airborne contaminants. The surfaces of the lotus of the planthopper are very different at the macroscopic level. Surprisingly, the topographic configuration is similar with micropillars of basal widths of 4–8 µm; 6–10 µm in height and spaced 14–20 µm apart (the smaller value of the range represents the planthopper and the larger value the lotus leaves). These features are less dense on the planthopper than in the lotus leaves. The nano-protuberance on the planthopper wing has a diameter of 47 nm while the wax tubules on the lotus leaf have a diameter of 100 nm. The water contact angle at the surface of the planthopper wing is 153°, very close to that of the lotus leaves. The micro-needles with nano-grooves induce the water repellence by the water striders (*Gerris remigis*) and enable water gliding.[44] The micro-setae are 50 µm in length, inclined at 20°, and covered by oriented nano-grooved waxes. The combination of hydroscopic wax and the hierarchical structure provides the water repellent property. Another example of superhydrophobic surface is found

in the thin and flexible membrane at the surface of the mosquito eye (*Culicidae* spp.). The eyes of mosquito contains thousands of lenses that are coated with pins of 100 nm in diameter and spaced 50 nm apart.[34] This nanostructure array feature air gaps that protect the surface from water. The green bottle fly (*Lucilia sericata*), desert beetle (*Physosterna cribripes*), and leafhopper (*Cicadellidae* spp.) have also documented micro- and nanostructure textured hydrophobic surfaces [45].

3. Properties of superhydrophobic materials

3.1. Wettability

The wetting phenomenon is very close to the adsorption phenomenon because they are both due to the interactions between the molecules of different substances[46]. If liquid molecules interact more strongly with the surface of the solid rather than the liquid, the latter will spread on the solid surface. This is the so-called wetting phenomenon. Wetting occurs only when the free energy of the system decreases. The lower the free energy, the better the wetting process. Upon wetting, the molecules in the droplet move on the surface of the solid in a manner that can reduce the surface tension. The phenomenon of wetting has various practical applications,[47-51] such as in froth flotation, protection of glue and emulsion, dyeing, construction, insecticides, and parasitoids.

In the case of superhydrophobic surfaces, the liquid molecules are more strongly attracted to each other than the interactions between the liquid and the solid surface to which they are exposed. When wetting does not occur, the liquid tends to condense to spherical drops. This is similar to a mercury droplet on the surface of a glass sheet or a solid non-metal surface. If the interactions between the liquid and the solid surface do not predominate, the wettability is imperfect. The latter will be determined by the degree of wettability expressed by contact angles.

3.2. Contact angle

The contact angle (CA) is the angle at the edge of the droplet with solid surface. The CA of a liquid droplet determines both the surface energy and the surface tension. Its value is determined by the tangent of the liquid droplet at the contact point between the solid, liquid and gas phases with the solid phase surface at the three-phase boundaries (**Figure 1**).

Figure 1

A liquid droplet perimeter is defined by the limit of three phases i.e. solid (S), liquid (L) and gas (G, often termed as vapor phase), which form the three separated interfaces, namely S-L, S-G and L-G. In 1805, Thomas Young described the equilibrium conditions on an ideal smooth surface as follows:

$$\gamma_{SG} = \gamma_{LS} + \gamma_{LG} cos\ \theta \quad (1)$$

where, γ is the surface tension, γ_{SG} at the S-G interface, γ_{LS} at the L-S interface, and γ_{LG} at the L-G interface. In practice, this equation is simplified to (Eq. 2), since the CA and the liquid surface tension can be measured readily.

$$\gamma = \gamma_L\ (cos\ \theta - 1) \quad (2)$$

From the Young's equation and the measured water contact angle (WCA), the wetting behaviour of a surface is generally classified according to the three categories shown in **Figure 2**[46] as follows: A hydrophilic surface has a WCA within $0° < \theta \leq 90°$; A hydrophobic surface has a WCA within $90° < \theta \leq 150°$, and when the WCA is within $150° < \theta \leq 180°$, the latter is called the superhydrophobic surface, where the sliding angle must be lower than 10°. A non-wetting surface has a WCA $\theta = 180°$. The CA varies with the liquid being measured. However, Vogler et al.[52] demonstrated that while considering the chemical and structural state of the water droplet, the division from

hydrophilicity and hydrophobicity should be 65° rather than 90°.[53] This division of hydrophobicity at 65° holds particularly for biomaterials, which exhibit both a chemical composition and a surface roughness that repels the water.

Figure 2

Experimentally, the contact angle of a liquid is determined by a tensiometer where the droplet of a liquid (water and organic solvents) is applied onto a solid surface using a micro-syringe. The size of the syringe, often made of polypropylene, could affect the droplet size, which may modify the CA values. The most common droplet size, used for CA measurements, is around of 10 µL. The image of the droplet is captured using a high-resolution camera. The CA value is then calculated by analysing the obtained image using a computer program that provides the tangent and the contact angle values. Another technique, named compressed droplets, is also used for measuring the wettability of a superhydrophobic coating surface. In this technique, a drop is compressed between two surfaces, among which at least one is textured (**Figure 3**). A force sensor makes it possible to measure the pressure on the drop. It also provides the anchoring forces of the liquid on the texture materials.[54-56] Following this approach, Lafumaet et al.[54] highlighted the transition phenomenon from Cassie-Baxter to Wenzel regime (**Figure 3a–3b**). They measured the pressure in the range of 100 to 300 Pa, and produced impingements of 10 µL of water droplets on the surfaces by triangular peaks with a height and width in the order of 2 mm. In the case of a texture surface produced by plasma etching and fluorination, Gnanappa et al.[57] evaluated the resistance to wetting of a texture by different liquids (**Figure 3c–3d**). By using compressed drops, Bormashenko et al.[58] highlighted the wetting transition from Cassie-Baxter to Wenzel by increasing the Laplace pressure of the drop during its evaporation (through the diminution of its radius).[59-61]

The Wilhelmy plate method[62-64] is a relatively simpler method of CA measurement. A clean metal sheet (mostly platinum) connected to a microbalance (sensibility of several mg) is withdrawn perpendicularly with measured interfaces (liquid-gas and liquid-liquid). The weight needed to remove the metal sheet from the defined interface is further used to calculate the surface energy according to the Ludwig Wilhelmy or Thomas Young model.[65]

There are many other techniques to determine the contact angle. Such methods include captive bubble method,[66] capillary rise at a vertical plate,[67] capillary tube,[68] capillary penetration method (for powders and granules[69]), capillary bridge method,[70] drop shape analysis,[71] axisymmetric drop shape analysis (ADSA),[72] and ultra-small droplets method.[73] In practice, the contact angle hysteresis (or dynamic contact angle) can be calculated using the difference between the exhibiting advancing (θ_a) and receding (θ_r) contact angles.

Figure 3

3.3. Surface roughness

Surface roughness and morphology allow the enhancement of superhydrophobic behavior of the materials.[33] Two key models of surface roughness can be used to explain the superhydrophobic effect. In the first model (the Wenzel model), they considered that the surface contact area was increased when the droplet penetrates into the asperities (**Figure 4**). The droplet contracts to avoid a large developed contact with the support, thereby increasing the contact angle.[31] According to the second model (the Cassie-Baxter model); the droplet rests on top of the asperities, which constitute the interface of the solid-liquid and solid-gas interface. The liquid cannot penetrate the porous surface and the hydrophobicity is consequently enhanced. While observing the natural superhydrophobicity, additional states are defined. In the lotus state, the asperities are also nanostructured. A transitional

state exists between the Wenzel and the Cassie-Baxter model. The "Gecko" state is a transitional state with partial wetting.

Figure 4

The Wenzel equation defines a roughness factor to consider the increased surface roughness from the asperities to emphasize the effect of the surface chemistry. The contact angle in the Wenzel state (θ_w) is defined according to Eq. 3. When $\theta > 90°$, an increase in roughness increases the θ_w, whereas for $\theta < 90°$, an increase in roughness reduces the θ_w.[33]

$$Roughness\ factor\ (r) = \frac{Actual\ surface\ area}{Planar\ surface} \quad (3)$$

According to the Cassie-Baxter's law,[74-76] the water droplets form spheres, and they reside on the top of the fibrous surface without filling in the nanoholes to maintain superhydrophobicity, which is further enhanced on microstructured and nanostructured fibrous surfaces. Equation 4 represents the Cassie-Baxter model:

$$\text{Cos}\ \theta_c = \varphi_1 \cos\theta_1 + \varphi_2 \cos\theta_2 \quad (4)$$

where, θ_1 is the contact angle of the substrate 1 occupied by a surface φ_1 (surface fraction of the phase 1) and θ_2 represents the contact angle of the substrate 2 occupied by a surface φ_2 (surface fraction of the phase 2). When the roughness is important, it is often assumed that the drop rests on a composite surface of solid and air, thus $\varphi_1 + \varphi_2 = 1$. In addition, when air is one of the media, the contact angle associated with this medium is 180°.

$$\text{Cos}\ \theta_c = \varphi_1 (\cos\theta_1 + 1) - 1 \quad (5)$$

where, φ_1 is the fraction of area occupied by the material. Eq. 5 implies that the materials with small surface fractions φ_1 and high contact angles θ_1 have superhydrophobic properties. In many applications,

277 it is preferable that the superhydrophobic materials should be stable and durable against acidic, basic
278 and solvent attacks.

279 The movement of the droplet on the contact line creates a CAH, which is the difference in
280 contact angle on the advancing contact line and the receding contact line.[77] The contact angle is greater
281 on the advancing line. The mobility is higher, and the adhesion is lower when the surfaces have a low
282 CAH. The contact angle hysteresis is measured by increasing and decreasing the volume of the droplet
283 with the sessile drop method and by measuring the contact angle on a tilted plane.[33] The tilting angle is
284 the angle just before the droplet starts to roll.

285

286 **3.4. Surface tension and surface energy**

287 The surface energy (γ) is considered as the energy needed to enlarge an interface between two
288 different phases of the surface unit without changing the volume of these phases. The molecules near
289 the surface do not have the same environment as volume. They are in contact with fewer molecules
290 than molecules in the bulk phase. The molecules at the surface have a higher potential energy (**Figure**
291 **5**). Solids tend to reduce their surfaces to minimize the zone of higher energy. A liquid droplet is
292 observed in a spherical form with the surface area/volume ratio at the minimum. The surface energy
293 and the surface tension usually have the same dimension.[78] The dimension of the surface tension is
294 both a force divided by the length (N/m or g/s^2) and a work by unit area (J/m^2 or g/s^2), which is a
295 surface energy.

296 **Figure 5**

297 The measurement of the surface energy of a liquid is straightforward because it is the same as
298 its surface tension (**Table 1**). The surface energy is a relative value because it cannot be directly
299 measured and must be calculated from a set of liquid/solid contact angles with liquids of known surface

tension. The value of the surface energy of the solid varies with the liquid selected.[79] Thus, the surface energy value is methodology-dependent and it can only be compared for the same measurement. For non-polar surfaces, the test liquid is non-polar, and the surface energy theory should not focus on the specific molecular interactions. In contrast, for polar surfaces, the test liquids must be polar, and the surface energy model should focus on the molecular interactions with 2–3 components to the surface energy. Non-polar interactions are attributed to dispersive forces (e.g. Van der Waals forces) and non-specific forces (hydrophobic interactions). Polar interactions are created with hydroxyl, carbonyl, amide and nitrate functional groups.

Table 1

4. Preparative methods for superhydrophobic nanocoatings

The two general rules for building superhydrophobic materials are tailoring the chemical composition and creating roughness on the surface.[53] The preparation methods based on the chemical nature are sol-gel, chemical etching, dip-coating and chemical deposition. The methods to enhance the surface roughness are physical etching and electrical deposition.

4.1. Sol-gel method

The sol-gel method is suitable to obtain high quality superhydrophobic coatings with good thermal resistance. This is considered as a complementary method to the physical and chemical deposition methods. However, this method exhibits several drawbacks involving crackability and thickness limits. The thermal treatment sometimes causes deteriorations in substrates. In principle, the sol-gel process is usually used to manufacture polymeric organic materials. However, in the case of the sol-gel pathway, a mineral polymerization resorts to molecular precursors in a solvent (alcohol or water) that is gradually transformed into a 3D network. This synthesis method often needs a thermal treatment at moderated time of a precursor to convert the materials on a specific surface by hydrolysis

and polycondensation reactions (also known as "soft chemistry"). This process allows depositing of superhydrophobic coatings on various substrates including metals, wood, glasses and ceramics. This method is now widely used to prepare superhydrophobic nanocoatings.[80-85] Superhydrophobic coatings prepared by sol-gel technique using silica nanoparticles derived from methyltriethoxysilane (MTEOS) have also been reported. The silica nanoparticles are initially mixed within the sol and then coated on the glass substrate. The superhydrophobic behaviour increases with nanoparticles content achieving a WCA of 162.5° and a pencil hardness of 5H.[85]

Xu et al.[86] have successfully synthesized a superhydrophobic cotton fabric by using chitosan/silica alcogel composites modified by 1H,1H,2H,2H-perfluorooctyltrimethoxysilane (PFOTMS) **(Figure 6).** By turning the preparative parameters, sponge-like nanoporous structure, entirely covered on cotton fabric, is obtained. The resulting cotton fabrics exhibit a high contact angles with various liquids such as water (164°), vegetable oils (160°) and hexadecane (156°). These coatings also have a good resistance to concentrated acid (98% H_2SO_4) and good mechanical properties that can withstand 10,000 cycles of abrasion and 30 cycles of washing without apparently changing the superamphiphobicity. Self-cleaning surfaces with double nanoscale textures are also prepared from an alumina sol using aluminum tri-sec-butoxide [$Al(O\text{-}sec\text{-}Bu)_3$], followed by a thermal treatment at high temperature[87].

Figure 6

Other approaches for achieving superhydrophobicity are to use methyltrimethoxysilane as raw material via a sol-gel method. The coating is prepared by dip-coating method onto glass plates. By this method, a WCA of about 170° is achieved and it maintained constant at about 550 °C.[88] One-step preparation of superhydrophobic coating is also reported by a sol-gel method where a perfluoroalkyl methacrylic polymer/fumed silica particle coating is provided on the fabric layers. The presence of

fluoropolymer leads to an oleophobic property of coating with contact angles of 146° and 113° for water and lubricant oil, respectively.[89]

More recently, Hao Zhang et al.[90] successfully synthesized a stable 3D sol-gel network coating having rapid self-healing ability. A branched thiol-enefluoroalkyl siloxane (T-FAS) was used to design a self-healing superhydrophobic 3D sol-gel network containing fluoroalkyl chain, the 1H,1H,2H,2H-perfluorodecyltriethoxysilane (FOTS). The coated fabric exhibited a high resistance to mechanical impacts (1000 cycles of abrasion under 45 kPa) and a good chemical resistance to strong acidic and basic solutions (e.g., H_2SO_4 and KOH), UV radiation, thermal treatment, and smudge treatment. The self-healing of the coating is expected due to a side-chain reorientation **(Figure 7).**[90] The dangling fluorinated chains were also protected by the durable 3D sol-gel networks.

Figure 7

Some transparent superhydrophobic coatings prepared by sol-gel methods have recently been reported in the literature.[91, 92] Other approaches to obtain a superhydrophobic coating have been described where the transparent resins such as polymethylmethacrylate (PMMA)[93] or 3-minopropyltriethoxysilane (APTS)[94] were mixed with a water repellent agent such as 1H,1H,2H,2H-perfluorooctyltrimethoxysilane; 1H,1H,2H,2H-perfluorodecyltrichlorosilane or methyl-trimethoxysilane. In this case, silica-based nanoparticles were used to make a rough coating surface.

4.2. Chemical and physical etching

In the nature, lotus leaves are considered as a model for the superhydrophobic surface. The structure of these leaves consists of two nano/micro-scale levels covered by natural waxes on the whole surface **(Figure 8a).** A lotus leaf has high superhydrophobic properties exhibiting a WCA higher than 160°. The surface of lotus leaves always remain clean even under mud and dirt.[95] The etching

technique is mainly bioinspired by this natural structure. The main objective is to increase the surface roughness of the substrate.

Figure 8

In an unpublished work, we have used the chemical wet coating method to create superhydrophobic cotton via chemical etching technique. Taking the advantage that cotton contains lignin and hemicellulose compounds (that can be chemically removed by the sodium hydroxide at moderate temperatures), it has been used for this purpose. By changing the treatment conditions, some soluble compounds such as lignin, waxes and low molecular weight molecules on the surface of cotton have been partially removed leading to a highly rough cotton surface. The latter is then treated with nanoparticles of silica at different concentrations. The esterification/etherification between hydroxyl groups on the silica nanoparticles can react with carbonyl and hydroxyl groups on the cotton surface at high temperatures and acidic catalysts to form a robust coating layer of nanoparticles. The coating is then covered by a hydrophobic agent (tetraethyl orthosilicate or TEOS) **(Figure 8c)** and finally a superhydrophobic cotton with a contact angle of 176° is obtained **(Figure 8b).** The schematic illustration in **Figure 8d** shows the final morphology of our superhydrophobic cotton. The main advantages of the chemical treatment are that it is inexpensive and simple. However, it brings some environmental challenges due to the use and generation of some toxic byproducts.

The removal of the outermost layers can be realized by physical etching. The main technique is plasma ablation.[96] This technique is comparatively simpler, cost-effective and environmentally friendly. The main principle is to use electrons to bombard the sample surface at a low pressure. This process is often conducted under oxygen atmosphere to crease the functional groups, which are later modified to a desired purpose. The main advantage of this method is that one can precisely select the treatment area. In other words, a selective treated surface can be obtained with plasma bombardments.

391 The treatment degree can be controlled by both treatment time and intensity of laser sources. For the
392 cotton fabric, the treatment time is found to be several tens of minutes.[97]

393 Water striders are other interesting examples of promising superhydrophobic surfaces, which have
394 special hierarchical set of arrays on their legs, making them capable of walking easily on the water surface.[98]
395 This property has inspired various researchers. For example, ribbed hair arrays-like materials were
396 synthesized by using a polymethyl methacrylate (PMMA) substrate with polystyrene (PS) sphere colloidal
397 lithography[99] followed by oxygen plasma reactive ion etching. The plasma treatments or electron irradiation
398 were performed to increase the WCA of various polymeric substrates such as polytetrafluoroethylene
399 (PTFE),[99, 100] polyimide (PI),[101] and fluorinated ethylene propylene (FEP).[102] The superhydrophobility is
400 increased with the treatment time, resulting in the PI becoming more hydrophilic while enhancing the
401 hydrophobicity of FEP. The contact angle in the optimum condition was about 150° with a good
402 mechanical stability.[103] In the case of PET, although the plasma ablation led to a significant change of
403 the surface morphology depending on the plasma treatment parameters, the WCA apparently decreased
404 with the treatment independent of time. The coating covered by perfluoroalkylsilane on the sample
405 surface showed a WCA of 160°.

406 The legs of water striders are also a typical example of naturally superhydrophobic structures due to
407 the presence of large nanoscale pillars covered by wax. This structure inspired the work by Wang et al.[99]
408 where the authors used a simple aquatic device to fabricate superhydrophobic hair arrays followed by coating
409 a PMMA in both surfaces. The resulting materials exhibited a good self-cleaning property and high-loading
410 capacity **(Figure 9)**, which was more than four times of their own weight. The large loading capacity[99] can
411 be due to the entire superhydrophobic coating in both the lower and the upper surfaces.

412 **Figure 9**

The plasma treatment has been successfully used to prepare submicrometer fibrils on the coating surface,[104] and a transition from Wenzel to Cassie-Baxter behavior is observed. In some special cases, some fluorinated-based gases, such as CF_4, C_2F_6, and SF_6, were used[105] instead of oxygen to induce superhydrophobic surfaces.[106] This technique imparts a rough surface and an in-road of water repellent compound in the sample surface.[107]

4.3. Dip-coating method

The dip-coating technique is widely used for the preparation of nanomaterials-based coating. It usually consists of two steps as discussed here. The first step relates to the soaking of a substrate in a solution containing nanoparticles and it's upwards pulling at a constant and controlled speed. The substrates are then covered by a water repellent agent after its removal from the solution. Due to the imposed pull-up rates, the nanocoating thickness on the substrate surface is also controlled. There are two pull-out rates of the substrate, which have direct effect on the thickness of the film.[108] At low pull-up rates in the capillary regime, the rate of evaporation of the solvent is greater than that of the shrinkage of the plate. This means that the shorter the shrinking speed, the thicker is the film. At high pull-up rates, the trend is reversed. In this so-called drainage regime, the combination of the adhesion of the solution to the substrate and the gravity forces the drainage of the solution. The advantage of this technique is that the preparation of a fast surface is therefore suitable for all forms of coated substrates. The fact that the solution can be reused until evaporation or depletion of the solute also makes this technique particularly convenient, especially for industrial applications.

Figure 10

Superhydrophobic sponge can also be prepared by dip-coating of silica nanoparticles (SiNP) followed by incorporation of a hexadecyltrimethoxysilane (HDTMS) (**Figure 10**). The

436 superhydrophobic mesh exhibits a WCA higher than 150° with oil separation efficiency of 95-99%
437 from wastewater/seawater mixtures. This material can withstand several cycles of the recycling tests.[109]

438 **4.4. Chemical and electrical deposition**

439 Electrodeposition (ED) is a conventional and low-cost method to create a thin layer of metals or
440 metallic alloys to a desired structure to modify its surface behaviour with various morphologies such as
441 needles, rods, ribbons, tubes, fibers and flower-like structures. The principle of this technique is to use
442 an electrical current to reduce the cations of the electrodeposited metals from electrodes to a conductive
443 surface. This method can be achieved at the room temperature and the coating becomes very stable
444 over time. The thickness of the coating can be easily tailored, which exhibits a low surface rugosity.
445 Electrodeposition is being considered as a main technology for massive production of the protective
446 coatings for large-area metallic protection, especially in the preparation of photovoltaics and solar
447 modules. In the case of polymeric materials, the electrodeposition consists of a monomer that is
448 oxidized in an electrochemical cell and polymerized to form a polymer for deposition on the electrode
449 surface. The textures are controlled by changing the deposition time and the current.

450 This method can be used to prepare various organic coatings such as polyethylene oxide (PEO),
451 polytetrafluoroethylene (PTFE)[110-112] and other organic matrices.[113-117] Various nanostructural organic-
452 inorganic coatings using electrophoretic deposition have been reported in the literature [140] such as
453 polyelectrolytes and poly(ethyleneimine). These were electrochemically deposited between the metal
454 ions and ceramic nanoparticles. The co-deposition by electrochemical method involving carbon
455 nanotubes and conducting polymers has also been studied[118-121]. Chitosan is reported as a dominant
456 organic matrix used for the electrodeposition of nanocomposite coatings.[122-124]

457 In practice, various superhydrophobic coatings are prepared by electrodeposition method. For
458 example, etched titanium substrate has been chemically deposited by a layer of 1H,1H,2H,2H-

perfluorooctyltrichlorosilane (PFOTS) to form a superhydrophobic coatings with high mechanical stability due to strong bonding between PFOTS and titanium.[125] A stable superhydrophobic film was also prepared by myristic acid. The contact angle was measured to be over 154°. An improved corrosion resistance of the coating in seawater was also observed.[125]

Repellent oleophobic coating prepared on stainless steel by using myristic acid, stearic acid ethanol and perfluoro-octanoic acid aqueous solutions are also reported. Superoleophobic coating exhibits a high contact angle (nearly 160° and 153° for deionized water and olive oil, respectively) with a low surface energy 0.60 mJ/m^2. The relationship between the surface properties, structure, chemical composition and mechanical properties was also investigated.[126] The development of superhydrophobic copper-based coatings using electrodeposition method is studied where a cauliflower shaped surface was first prepared followed by the treatment with stearic acid. The elaborated coatings exhibited a contact angle of 162±2° and presented a good mechanical durability. The coatings also possessed high performance, underwater stability, corrosion resistance and self-cleaning effects.[127] Zhang et al.[128] showed a cost-effective route to prepare a superhydrophobic surface by electrodepositing the solution containing cerium nitrate hexahydrate - myristic acid. Before the electrodeposition step, the substrate was polished by electrochemical method using perchloric acid and ethanol solution. The cerium (III) nitrate hexahydrate and myristic acid in ethanol were employed as the electrolyte at room temperature (**Figure 11**). The resulting surfaces had a contact angle higher than 162°. The electrochemical impedance spectroscopy (EIS) confirmed that the synthetized surface significantly enhanced the corrosion resistance up to three orders of magnitude compared to the initial aluminum substrate.[128] In a similar study, Beshkar et al. demonstrated the formation of CuO/ZnO hybrid hierarchical nanostructures growing on copper oxide foils via a glycothermal method (Beshkar et al., 2017). These nanostructures had a flower-like morphology and exhibited hydrophobic and anticorrosion properties.

Figure 11

4.5. Other techniques

Other techniques employed to prepare superhydrophobic coatings include spraying, chemical vapor deposition, spin-coating, photochemistry, lithography and electrospinning.[33] The choice of a suitable preparation method depends on the end-use application. Each method has its own advantages and drawbacks. For example, the spray method is suitable for treated surfaces and exterior applications. However, the contact angle is hardly 160°; thus, this method is used for textiles, construction and glass applications. In contrast, superhydrophobic coatings prepared by spin-coating presents a low rugosity with a precision thickness. However, it is suitable for small surfaces. The lithography is demanding, which is a complicated procedure making it difficult to implement at the industrial scale.

5. Promising applications of superhydrophobic coatings

With numerous interesting properties mentioned previously, the range of application of superhydrophobic coatings is deemed very large.[12, 129-132] Several key applications (with the required performance features) are listed in **Table 2.**

Table 2

5.1. Self-cleaning

Self-cleaning is an interesting property of coating materials. This phenomenon relates to the removal of dirt from the coating surface and can be used for various applications. There are two main strategies to achieve to this self-cleaning attribute. The first strategy is to use photocatalytic additives, which can decompose organic pollutants under light. The most common photocatalysts are TiO_2 and related compounds. The second approach is to design the surface of the coating to impart hydrophilic

503 or hydrophobic property.[133] The increase of roughness of the surface is crucial for self-cleaning
504 properties.

505 Photocatalytic and superhydrophobic strategies can be simultaneously used for the self-cleaning
506 property of nanostructured materials. Recently, Najafian et al. (2019) have fabricated a nanocomposite
507 photocatalyst $CuBi_2O_4/Bi_3ClO_4$ via an improved Pechini sol-gel process using mixtures of many
508 gelling agents and polybasic acids. The nanocomposite photocatalysts demonstrated the removal of
509 acid brown 14, a water pollutant, under visible light irradiation. Najafian et al. (2018) have also
510 reported a novel and facile approach of preparing $ZnBi_{38}O_{58}$ nanostructures using the amino acid-
511 assisted sol-gel combustion route also involving various gelling agents. The $ZnBi_{38}O_{58}$ nanostructures
512 having spherical, plate-like, cubic and polyhedral morphologies demonstrated efficient degradation of
513 azo dye pollutants under visible-light irradiation. Similarly, synthesis of a novel and photocatalytic
514 $NiO/Bi_2O_3/Bi_3ClO_4$ nanocomposite for the degradation of azo dye pollutants under visible light
515 irradiation has been reported (Najafian et al. 2019).

516 In practice, transition oxides are commonly used for designing a nanoscale rough surface. For
517 example, ZnO is used to prepare nanorod surfaces with self-cleaning behaviour **(Figure 12a–12d),**
518 while self-cleaning flower-like structures are synthesized from aluminum foils **(Figure 12e–12f).** The
519 self-cleaning properties exhibit similar principles. Zeng et al.[134] have shown a facile and low-cost
520 approach to prepare self-cleaning superhydrophobic surfaces using zeolite coated by an ethanoic
521 suspension of perfluorodecyltrichlorosilane. The etching of the glass micro-slides and plastic holder
522 substrates are carried out by oxygen plasma etching. This helps not only to remove surface impurities
523 and contaminants but also create activated species on its surface. These substrates are then treated with
524 an octadecyltrichlorosilane (ODTS) solution of around 0.2 M drop-by-drop. The prepared coatings
525 show exhibits both water and oil repellent properties with high mechanical resistance.[134]

Figure 12

Ding et al. showed some interesting results on the preparation of the superhydrophobic self-cleaning fluorinated polysiloxane/TiO_2 coatings.[135] Cataldi et al.[136,] and Bayer et al. [137] have published several articles on the preparation of superhydrophobic coatings for various applications. The synthesis of a multifunctional coating, which exhibits both the self-cleaning and anti-glare properties with a high WCA (168°) is also reported. These prepared coatings are very stable in terms of self-cleaning property in outdoor conditions (up to 2000 h of exposure).[138]

Li et al.[139] reported a synthesis of superhydrophobic multi-wall carbon nanotubes (MWCNT) based nanocomposites and a thermoplastic elastomer (TPE). These smart coatings can be easily prepared at ambient conditions without surface treatment of the substrate. The coating superhydrophobic behaviour remains irrespective of the various substrates. These coating also exhibits a good resistance to UV radiation and chemical attacks, which is suitable for the preparation of superhydrophobic coated flexible materials. More recently, Zhang et al.[140] synthesized superhydrophobic surfaces by a green approach and coated in the stainless steel meshes for filtration purpose. The authors showed that the as-prepared coating can stand upto 50 cycles with sandpaper and high efficient oil/water filtration.[140]

5.2. Anti-biofouling

When an object (substratum) is immersed in seawater, microorganisms (bacteria and protozoa), benthic organisms (diatoms), and nanoparticles are attached onto its surface and finally forming a biofilm.[141] The object develops a complex structure composed of a consortium of microorganisms, which multiply and gradually cover the surface with the biofilm. The effects of bio-fouling cost marine, shipping and other global industries billions of dollars every year.[142] The biofilm can change the morphology of the substratum and lead to corrosion of metals. The anti-fouling coating is to prevent

549 the development of biofilms with and without biocide.[142] The anti-fouling coating can be categorized
550 into two classes such as self-polishing coating (SPC) and fluorine-based coating (FRC). An effective
551 anti-fouling coating should include properties such as durability, good adhesion, corrosion inhibition,
552 smoothness, easy application, fast drying, low-cost and easy availability. Tributyltin (TBT) has been
553 used as an anti-fouling agent.[143, 144] The anti-fouling coating is often mixed with toxic components such
554 as Pb^{+} to inhibit microbial biofilm formation. However, the release of the toxic compound into the
555 ecosystem makes anti-fouling agents challenging to use in the marine environment. Recently,
556 superhydrophobic coating has emerged as a suitable candidate for the fouling coating. Fluorine-based
557 coating fails to prevent colonization of biofilm but inhibits the adhesion of fouling under almost all
558 dynamic conditions. **Figure 13** shows a typical approach of marine anti-fouling coating.

559 **Figure 13**

560 The anti-fouling membrane shown in this figure is based on phosphorylcholine (PC) and
561 adhesive catechol (C), grafted at the amino-ends of an 8-armed poly (ethylene glycol). The authors
562 argued that the random grafting of PC co-polymer and incorporated ester groups increase the catechol.
563 Pre-coating the substrate with polydopamine leads to an enhancement of anchoring interaction. The
564 latter is automatically formed from a dopamine solution onto almost all substrates including
565 polytetrafluoroethylene.[145]

566 A biodegradable poly-(ε-caprolactone)-based polyurethane has also been used to prepare
567 superhydrophobic coatings. It was indicated that the polymer degradation rate appears to increase with
568 the presence of marine organisms or enzymes. The release rate of butenolide (a potent anti-fouling
569 agent) depends on both the temperature and the initial concentrations and the duration of this release is
570 about three months. The addition of a natural resin (rosin) into the biodegradable formulation leads to
571 an increase in the self-renewal and the release rate of butenolides.

Recently, fouling self-cleaning coatings have been synthesized through salt spray tests. The author argued that the prepared coating exhibited low surface free energy and rugosity leading to an efficiency inhibition of the fouling settlements. The incorporation of only 0.5% ZnO-SiO_2 nanospheres helped minimize the surface tension and thus improved fouling resistance. These coatings also exhibited good mechanical and anti-corrosive properties in aqueous salt fog environments. Some models of biological foulant for biofilm formation such as bacteria (*Micrococcus* sp. and *Pseudomonas putida*) and fungi (*Aspergillus niger*) have been investigated. The coating showed inert and superhydrophobic properties with a contact angle of 165±2° along with high thermal stability, good durability under UV radiation and high resistance against various pH solutions. [146]

5.3. Anti-bacterial feature

The need for anti-bacterial coatings has recently drawn a great attention among the researchers due to its large potential application in various fields, especially in public areas where the bacterial risk is high. Therefore, the development of controlled release strategies is crucial to control the biological activity of the coating.[147] The most common method for anti-bacterial coating is to use silver nanoparticles and its derivatives. Silver nanoparticles (AgNPs) are reported to have high anti-bacterial properties that can kill various microorganisms. The biological activity of AgNPs can be improved by reducing their particle size and modifying their surfaces. However, the most recent strategy for increasing the anti-bacterial activity of AgNPs includes the combination of AgNPs with other oxides such as nanosilverferrite composite. Heinonen et al.[148] investigated the anti-bacterial activity of superhydrophobic coatings containing silver nanoparticles at different pH solutions. Recently, a method to prepare multifunctional silk has also been developed. The silk was coated a superhydrophobic layer using large water repellent compounds and silica nanoparticles. This obtained a multifunctional material having anti-microbial properties with superhydrophobic and superoleophobic

properties (contact angle >150°) against water and oil. The protective coating hinders the development of the bacteria and microorganisms on the coated silk.[149]

Figure 14

He et al.[150] prepared contact-active anti-bacterial surfaces by using a quaternary ammonium salt waterborne polyurethanes (GWPU) containing an anti-fouling agent based on polyethylene glycol/lysine. The prepared coating showed an excellent biological property to bacterial contamination of artificial surfaces **(Figure 14).** The coating demonstrated a reversed surface structure integrated with the anti-bacterial upper-layer and the anti-fouling sub-layer. The anti-bacterial activity of the upper-layer and anti-fouling attributes of the sub-layer led to an enhancement of the coating surface. The growth of both Gram-positive and Gram-negative bacteria is inhibited after coming in contact with these anti-fouling coatings.[150]

5.4. Anti-icing

Anti-icing is one of the most interesting properties of superhydrophobic coatings, which can greatly eliminate many of the effects of ice storms and aircraft icing. In the literature, these coatings are sometimes called ice-phobic coatings. Anti-icing is well-known and very complex. The understanding of these phenomena requires a multidisciplinary acknowledge as they relate to: (i) interactions between the water and the solid surface, (ii) ice nucleation mechanisms, and (iii) ice adhesion parameters. Superhydrophobic coatings exhibit low interfacial energy and reduce the ice adhesion. The latter is important to remove the ice by external mechanical force easily. A detailed description on anti-icing can be found in several recent review articles[77, 151] where various fabrication methods for ice-phobic coating are presented (**Figure 15**). Most of the developed approaches relate to the reduction strength of adhesion force between the ice and the substrates. For example, Ozbay et al. have used self-lubricating features to prepare ice-phobic coatings with low ice adhesion strength.[152]

Figure 15

Drag reduction, a property also bioinspired by lotus leaves, is found to be associated with hydrophobicity. Aircrafts and submarines often encounter challenges relating to drag. On superhydrophobic coatings, a gas film is formed between the water and the coated surface, which reduces the contact between the solid substrate and water.[153, 154]

5.5. Superoleophobicity

Superhydrophobic surfaces are often wetted by oil and other liquids with lower surface tension (surface tension of water is 20–60 N/m compared to that of 2 nN/m for oil.[53] Superoleophobic materials are rare in nature. Materials exhibiting both superhydrophobic and superoleophobic properties are rapidly emerging.[155] The chemical composition with versatile fluorinated polymer increase the superoleohydrophobicity but remains challenging in industrial manufacturing. Different morphologies allow increasing the oil repellency. The wettability of a material can be selectively controlled by selecting the reagent. For example, kaolin was rendered superhydrophobic in a procedure in stearic acid and ethanol, superoleophobic with perfluorooctanoic acid and sodium hydroxide. Superoleophobic surfaces can also have anti-bacterial, anti-reflection, corrosion resistance, oil capture and oil transport, oil/water separation, self-cleaning, and more properties.[155]

5.6. Specific applications in solar cells

In addition, superhydrophobic coatings play a vital role in designing solar panels that has emerged as one of the most promising sustainable energy for urban and rural housing. The efficiency of solar energy systems is greatly influenced by the amount of radiation incident on the photovoltaic (PV) cells. In a solar panel, the array of silicon solar cells is placed behind the glass. The glass often becomes dirty due to various environmental factors, which highly affects the efficiency of the solar cells in harnessing the sunlight.[156] Cleaner solar panels yield more energy when compared to soiled

panels. Pavan et al. reported a 6.9% power loss due to the pollution caused by a plant located on a sandy site in the southern Italy.[157] According to El-Shobokshy and Hussein, fine dust particles decrease the efficiency of the photovoltaic cells while significant reduction in efficiency is caused by the coarse particles.[158] Sarver et al.[159] reported that the dust decreases the energy output in both the photovoltaic cells and concentrating solar power systems. They also reported that solar intensity reaching the solar panel is typically reduced in the range of 20–50%, which consequently decreases the power output from the photovoltaic system by 15–30% in an average dust condition.[159] Concentrating solar panels (CSP) are more sensitive to dust adhesion as soiling causes more adverse effects on the reflective surfaces. Even a small decrease in surface reflectivity due to soiling on the reflective mirrors would result in a great loss in CSP energy output. Some other factors such as partial shading by soil patches, fallen leaves, bird droppings etc. may also block some photovoltaic cells of a module. These shaded cells are unable to produce power; hence, act as a resistance and cause heating to form hotspots, which could potentially damage the solar panels.[160, 161] Damaged panels due to the formation of hotspots are shown in **Figure 16**.

Figure 16

It is clear from the above discussions that the cleaning and maintenance of a solar panel is an essential task, which must be performed with priority to enhance the efficiency of the photovoltaic cells. Numerous cleaning methods have been suggested for solar panels. Such methods include manual cleaning, cleaning from natural sources and mechanical cleaning such as using wipers, robotic arms, etc. Cleaning of solar panel usually requires large amount of water and manpower, which make maintenance a costly operation. In addition, repeated cleaning by scrubbing the solar panels creates scratches on the panel, which increases reflections of solar light from the top glass cover. Many researchers have reported that superhydrophobic coatings on solar panels are capable of self-cleaning.

When the water droplets fall on a superhydrophobic surface, they roll down collecting the dust particles with them.[162-164] Collection of dust particles by rolling of water drops on the glass surface is a beneficial feature for overall efficiency increase of a solar plant. Nanostructured superhydrophobic coatings have been extensively used to make glass surfaces dust-repellent and making them easier to clean.

Developing superhydrophobic coating for solar panels is not an easy task as the transparency of the glass cannot be compromised. For solar panel applications, the coating should be highly transparent. Creating anti-reflectivity with superhydrophobic material is an added advantage. Gwon et al.[165] produced nanograss-coated superhydrophobic (SNGC) glass surfaces with both reduced reflectivity and improved self-cleaning properties. Park et al.[166] fabricated microshell array in a perfectly ordered manner on a polydimethylsiloxane (PDMS) substrate for solar cell application. They evaluated and demonstrated the self-cleaning behaviour of the PDMS with microshell and compared it with a plane PDMS substrate without microshell on the photovoltaic cell. They found a superior self-cleaning efficiency by the microshell PDMS surface.[166] Quan and Zhang[167] developed a transparent hydrophobic coating on solar cells using tetraethoxysilane (TEOS) with SiO_2 nanoparticles and evaluated its anti-dust effects. They found a lower adhesion force between the dust particles and the surface. Ji et al.[167] fabricated stable superhydrophobic glass surfaces by one-step hydrothermal method with vinyltriethoxysilane. It was found that the fabricated surface was highly superhydrophobic with contact angle of 155° and sliding angle of 5°.[167]

Liu et al.[168] fabricated hierarchically structured coatings on a glass substrate by an one-step hydrothermal method. The coated surfaces were found to be rough having flower-type particles arranged by nanoflakes or urchin-type particles made by nanowires. The coated glass was further treated with 1H,1H,2H,2H-perfluorooctyltriethoxysilane for surface modification to create

superhydrophobicity. After treatment, the contact angle was found to be 160°.[169] Amorphous aluminum oxide coatings with an interconnected porous network of nanoflakes on glass substrate were developed for solar applications.[170] Sutha et al. also used zinc oxide (ZnO) to fabricate superhydrophobic surfaces on a glass substrate previously seeded with aluminum oxide. Nanowall-like morphology was found on the ZnO bad coating.[170] For preparing transparent superhydrophobic coatings, various low surface energy materials are normally used. Silanes are very common low surface energy materials used for preparing highly transparent superhydrophobic coatings.

Alkylsilanes are very common precursor used in the sol-gel method for the preparation of transparent superhydrophobic coating. Silanes are silicon chemicals having a hydrolytically sensitive center that can form stable covalent bonds by reacting with inorganic substrates such as glass. They also have an organic substitution that is responsible for the physical interactions with the substrates. To make a substrate surface hydrophobic, the hydroxyl groups present on the substrate should be removed or capped. Organosilanes effectively eliminate hydrogen from hydroxyl group by forming oxane bonds. Therefore, non-polar substitution by silane shields the polar substrate from interacting with water. The treatment by silane depends on the number of hydroxyl groups on the substrate. Methylsilane, linear alkysilane, branched alkylsilane, arylsilane, and dipodal silane are the main classes of hydrophobic silanes used in the modification of surface energy to create superhydrophobic effects on a glass substrate. Tetraethoxysilane (TEOS) is the most common alkylsylane used for the preparation of transparent superhydrophobic coatings.[167, 171] Fluoroalkylsilanes (FAS) are commonly used low-surface-energy materials for fabrication of a superhydrophobic surface. A hydrophobic fluoroalkyl group is present at the tail end and it assembles itself as a monolayer on a solid surface by orienting its molecular axis perpendicular to the substrate surface.[172]

Xiu et al.[173] developed porous and rough sol-gel silica coatings by using templating agents. The coating was then modified by FAS to impart superhydrophobicity. Li et al.[174] fabricated a hierarchically porous silica surface that was made superhydrophobic by surface modification using FAS. FAS is also utilized as a co-precursor in the sol-gel method to develop superhydrophobic materials.[175, 176] FAS is mostly used in combination with other precursors. Only a few researchers have reported the use of FAS as a precursor without combining them with other agents to produce superhydrophobic surfaces.[177] (Heptadecafluoro-1,1,2,2-tetrahydrodecyl) trimethoxysilane or HDFTS,[178] tridecafluoro-1,1,2,2-tetrahydrooctyltrichlorosilane (FOTS)[179] and 3-(2,2,3,3,4,4,5,5-octafluoropentyloxy) propyltriethoxysilane (OPF)[180] are some commonly used fluorosilane precursors. Other than silanes, some hydrophobic polymers such as perfluorocyclobutane and poly(P-phenylene butylenes) are also used for the preparation of self-cleaning superhydrophobic transparent coatings on concentrated solar power systems.[181] Many nanocoating companies are developing superhydrophobic coatings for solar panels. Nanopool® GmbH (Germany), Nano Shell Ltd (UK) and NanoSonic Inc. (USA) are some leading companies.[182] Moreover, superhydrophobic coatings featuring self-cleaning, anti-dust, anti-mist properties are of prime significance in promoting the performance of optical applications such as light luminance, photon crystals and solar cells.[125]

Table 3

5.7. Applications in fuel cells and electronic devices

Superhydrophobic materials can enhance durability and efficiency of fuel cells, batteries, supercapacitors and other electronic devices. Lifton et al.[183] demonstrated the use of silicon materials modified with superhydrophobic nanostructures in the electrodes of a battery. The superhydrophobic coatings resulted in effective separation of the liquid electrolyte from the electrodes, thus preventing the chemical reaction from taking place. Electrowetting changes the wetting and contact angle of the

liquid electrolyte on the superhydrophobic electrodes upon activation of the battery and potential difference between the solid electrode and liquid electrolyte. This could significantly extend the shelf life of the battery.

In fuel cells, carbon nanotubes in superhydrophobic orientation as cathode catalyst with Pt nanoparticles have shown improvement in the overall efficiency.[184] Superhydrophobic carbon nanotubes were found to repel water produced during the electrode reaction off the electrode to improve the mass transport in the fuel cell. This water repellency attribute of superhydrophobic coatings have also led to research on waterproof coatings on moisture-sensitive electronic devices, probes and sensor chips resulting in the elimination of the surface discharge caused by the leakage current at high humidity.[185]

5.8. Superhydrophobic fabrics and textiles

The application of superhydrophobic coatings can also be extended to manufacture fabrics and textiles with excellent water-repellency. Superhydrophobic textiles can be generated by weaving low surface energy fabrics having micro- or nanostructures.[185] The super water repellency property together with low tilt angle of water droplets in engineered fabrics imparts superhydrophobic and self-cleaning properties to woven textiles. Such modifications can change the wetting property of textiles while retaining comfort, warmth, softness and fabric-specific properties such as non-toxicity, crease-free, durability, etc. Ma et al.[186, 187] fabricated poly(caprolactone) (PLC) and poly(styrene-block-dimethylsiloxane) copolymer fibers using combined electrospinning and chemical vapor deposition techniques. PCL was electrospun, followed by thin-layer coating of hydrophobic polymerized perfluoroalkyl ethyl methacrylate (PPFEMA) by chemical vapor deposition. The prepared PPFEMA-coated PCL composite exhibited both oleophobicity and hydrophobicity. The hydrophobicity was

found to increase gradually with a decrease in the diameter of high-density bead-free fibers, which determine the wetting property.

One of the emerging applications of superhydrophobic and superoleophobic textiles is found in military, firefighting, and other defense-related occupations. However, the performance, assessments tests, durability, physico-mechanical properties, chemical resistance, and personal comfort related to the superhydrophobic fabrics and textiles determine their applications in such challenging real-world situations.[188] Most countries are concerned about the military requirements to protect their soldiers from being wet with water or chemicals on the line of defense or during missions in chemical or biohazardous environments.

The robustness and performance factor of superhydrophobic materials in an outdoor environment under extreme conditions is often questionable. Engineering the surfaces for maintaining low surface energy or phobic properties to attain long-term superhydrophobicity is also challenging. External factors such as chemical attack, sun bleach as well as mechanical wear and tear (e.g., friction, rubbing, scratches, and abrasion) can low the surface energy.[125] However, nanostructured superhydrophobic polymeric materials with self-healing property and long-lasting robustness is highly promising. With self-healing property, the polymeric material can restore the damaged surface and retain its superhydrophobicity while maintaining low surface energy.[189] Research efforts are being invested to impart self-healing attribute to the polymeric surfaces, fiber geometry, diameter and density and weave structure of superhydrophobic textiles to obtain enhanced liquid non-wetting properties.[190]

6. Conclusions

This review paper provided an overview of the literature pertaining to the superhydrophobic nanocoatings. Firstly, we discussed the fundamental aspects of wettability and surface tension phenomena, followed by a thorough discussion on the preparation methods and key areas of application

of superhydrophobic coatings. Some new developments on the etching method are also discussed. The advantages and drawbacks of each method have been identified. In general, to obtain a superhydrophobic surface, the rugosity of the surface plays a key role. The implication of a water (or oil) repellent compound is also essential to achieve an efficient superhydrophobic or superoleophobic surface. In some special applications, other additives are needed to achieve the final goal. For example, a biocide is added in the superhydrophobic nanocoatings to increase the efficiency of microbial biofilm removal. In the case of anti-icing coating, some anti-ice nucleating agents are needed to reduce the adhesion strength between the ice and the protective surface. Optically transparent and highly stable superhydrophobic coatings have promising application in solar cells to protect them against environmental effects, such as UV, heat, and humidity.

Future works should focus on the improvement of the durability of the superhydrophobic coatings, especially in laundering resistance to expand their application in flexible materials. Although various investigations showed the successful synthesis of high resistance superhydrophobic coatings against mechanical attacks, the laundering effect is scarcely reported. Moreover, the self-healing properties as well as the corrosion protection features should be considered for the preparation of superhydrophobic coatings. To deploy them in a large-scale, researchers need to find eco-friendly, cost-effective and scalable methods to prepare this interesting class of materials. Investigations should also focus on the design and preparation of superhydrophobic coatings for use in advanced fields, such as in sustainable energy production and storage.

Appendices

SHCs	Superhydrophobic coatings
CAH	Contact angle hysteresis

800	CA	Contact angle
801	WCA	water contact angle
802	S	Solid
803	L	Liquid
804	G	Gas
805	γ	Surface tension
806	γ_{SG}	Surface tension at the solid-gas interface,
807	γ_{LS}	Surface tension at the liquid-solid interface,
808	γ_{LG}	Surface tension at the liquid-gas interface
809	θ_1	Contact angle of the substrate 1 occupied by a surface φ_1
810	θ_2	Contact angle of the substrate 2 occupied by a surface φ_2
811	MTEOS	Methyltriethoxysilane
812	PFOTMS	1H, 1H, 2H, 2H-perfluorooctyltrimethoxysilane
813	$Al(O\text{-}sec\text{-}Bu)_3$	Aluminum tri-sec-butoxide
814	MTOS	Methyltrimethoxysilane
815	PMP	Perfluoroalkylmethacrylic polymer
816	T-FAS	Thiol-enefluoroalkyl siloxane
817	FOTS	1H, 1H, 2H, 2H-perfluorodecyltriethoxysilane
818	PMMA	Polymethylmethacrylate
819	APTS	3-minopropyltriethoxysilane

820	TEOS	Tetraethyl orthosilicate
821	PS	Polystyrene
822	PTFE	Polytetrafluoroethylene
823	PI	Polyimide
824	FEP	Fluorinated ethylene propylene
825	CF_4	Tetrafluoromethane
826	C_2F_6	Hexafluoroethane
827	SF_6	Sulfur hexafluoride
828	SiNPs	Silica nanoparticles
829	HDTMS	Hexadecyltrimethoxysilane
830	ED	Electrodeposition
831	PEO	Polyethylene oxide
832	PFOTS	1H, 1H, 2H, 2H-perfluorooctyltrichlorosilane
833	EIS	Impedance spectroscopy
834	TiO_2	Titanium dioxide
835	ZnO	Zinc oxide
836	ODTS	Octadecyltrichlorosilane
837	MWCNT	Multiwalled carbon nanotubes
838	MSHOs	Multifunctional superhydrophobic and superoleophilic surfaces
839	SPC	Self-polishing coating

FRC	Fluorine-based coating
TBT	Tributyltin
PC	Phosphorylcholine
PCL	Poly-(ε-caprolactone)
AgNPs	Siver nanoparticles
GWPU	Waterborne polyurethanes
PV	Photovoltaic cells
SNGC	Nanograss-coated superhydrophobic
PDMS	Polydimethylsiloxane
HDFTS	(Heptadecafluoro-1,1,2,2-tetrahydrodecyl) trimethoxysilane
TFOTS	Tridecafluoro-1,1,2,2-tetrahydrooctyltrichlorosilane
OPF	3-(2,2,3,3,4,4,5,5-octafluoropentyloxy) propyltriethoxysilane

References

1. M. L. Zheludkevich, D. G. Shchukin, K. A. Yasakau, H. Möhwald and M. G. S. Ferreira, *Chemistry of Materials*, 2007, **19**, 402-411.
2. H. Abdollahi, A. Ershad-Langroudi, A. Salimi and A. Rahimi, *Industrial & Engineering Chemistry Research*, 2014, **53**, 10858-10869.
3. L. Yan, Y. Xiang, J. Yu, Y. Wang and W. Cui, *ACS Applied Materials & Interfaces*, 2017, **9**, 5023-5030.
4. S. Rtimi, R. Sanjines, C. Pulgarin and J. Kiwi, *ACS Applied Materials & Interfaces*, 2016, **8**, 47-55.
5. T. Nardi, S. Rtimi, C. Pulgarin and Y. Leterrier, *RSC Advances*, 2015, **5**, 105416-105421.
6. S. Rtimi, S. Giannakis and C. Pulgarin, *Molecules*, 2017, **22**.
7. A. Bonnefond, E. Gonzalez, J. M. Asua, J. R. Leiza, J. Kiwi, C. Pulgarin and S. Rtimi, *Colloids Surf B Biointerfaces*, 2015, **135**, 1-7.
8. J. Hoque, P. Akkapeddi, V. Yadav, G. B. Manjunath, D. S. S. M. Uppu, M. M. Konai, V. Yarlagadda, K. Sanyal and J. Haldar, *ACS Applied Materials & Interfaces*, 2015, **7**, 1804-1815.
9. Z. Zhi, Y. Su, Y. Xi, L. Tian, M. Xu, Q. Wang, S. Padidan, P. Li and W. Huang, *ACS Applied Materials & Interfaces*, 2017, **9**, 10383-10397.
10. S. Guldin, P. Kohn, M. Stefik, J. Song, G. Divitini, F. Ecarla, C. Ducati, U. Wiesner and U. Steiner, *Nano Letters*, 2013, **13**, 5329-5335.
11. B. Stieberova, M. Zilka, M. Ticha, F. Freiberg, P. Caramazana-González, J. McKechnie and E. Lester, *ACS Sustainable Chemistry & Engineering*, 2017, **5**, 2493-2500.
12. S. Das, S. Kumar, S. K. Samal, S. Mohanty and S. K. Nayak, *Industrial & Engineering Chemistry Research*, 2018, **57**, 2727-2745.
13. W. Wang, K. Lockwood, L. M. Boyd, M. D. Davidson, S. Movafaghi, H. Vahabi, S. R. Khetani and A. K. Kota, *ACS Applied Materials & Interfaces*, 2016, **8**, 18664-18668.
14. S. Atiganyanun, J. B. Plumley, S. J. Han, K. Hsu, J. Cytrynbaum, T. L. Peng, S. M. Han and S. E. Han, *ACS Photonics*, 2018, **5**, 1181-1187.
15. Z. Xing, S.-W. Tay, Y. H. Ng and L. Hong, *ACS Applied Materials & Interfaces*, 2017, **9**, 15103-15113.
16. J. Kiwi and V. Nadtochenko, *The Journal of Physical Chemistry B*, 2004, **108**, 17675-17684.
17. S. Rtimi, C. Pulgarin, V. A. Nadtochenko, F. E. Gostev, I. V. Shelaev and J. Kiwi, *Scientific Reports*, 2016, **6**, 30113.
18. S. Rtimi, C. Pulgarin, M. Robyr, A. Aybush, I. Shelaev, F. Gostev, V. Nadtochenko and J. Kiwi, *Applied Catalysis B: Environmental*, 2017, **208**, 135-147.
19. I. Milosevic, S. Rtimi, A. Jayaprakash, B. van Driel, B. Greenwood, A. Aimable, M. Senna and P. Bowen, *Colloids Surf B Biointerfaces*, 2018, **171**, 445-450.
20. L. Kong, X. Yin, Y. Zhang, X. Yuan, Q. Li, F. Ye, L. Cheng and L. Zhang, *The Journal of Physical Chemistry C*, 2013, **117**, 19701-19711.
21. P. Li, K. Sun and J. Ouyang, *ACS Applied Materials & Interfaces*, 2015, **7**, 18415-18423.
22. M. Przybylak, H. Maciejewski, A. Dutkiewicz, I. Dąbek and M. Nowicki, *Cellulose*, 2016, **23**, 2185-2197.

23. L. Xiao, M. Deng, W. Zeng, B. Zhang, Z. Xu, C. Yi and G. Liao, *Industrial & Engineering Chemistry Research*, 2017, **56**, 12354-12361.

24. L. Cao, A. K. Jones, V. K. Sikka, J. Wu and D. Gao, *Langmuir*, 2009, **25**, 12444-12448.

25. P. Chevallier, S. Turgeon, C. Sarra-Bournet, R. Turcotte and G. Laroche, *ACS Applied Materials & Interfaces*, 2011, **3**, 750-758.

26. C.-C. Chang, F.-H. Huang, H.-H. Chang, T.-M. Don, C.-C. Chen and L.-P. Cheng, *Langmuir*, 2012, **28**, 17193-17201.

27. R. Mohammadi, J. Wassink and A. Amirfazli, *Langmuir*, 2004, **20**, 9657-9662.

28. X. Kong, J. Zhang, Q. Xuan, J. Lu and J. Feng, *Langmuir*, 2018, **34**, 8294-8301.

29. Z. Lu, Z. Chen, Y. Guo, Y. Ju, Y. Liu, R. Feng, C. Xiong, C. K. Ober and L. Dong, *ACS Applied Materials & Interfaces*, 2018, **10**, 9718-9726.

30. I. A. Makaryan, I. V. Sedov and P. S. Mozhaev, *Nanotechnologies in Russia*, 2017, **11**, 679-695.

31. T. Darmanin and F. Guittard, *Materials Today*, 2015, **18**, 273-285.

32. H. Zhu, Z. Guo and W. Liu, *Chemical Communications*, 2014, **50**, 3900-3913.

33. E. Celia, T. Darmanin, E. Taffin de Givenchy, S. Amigoni and F. Guittard, *Journal of Colloid and Interface Science*, 2013, **402**, 1-18.

34. T. B. H. Schroeder, J. Houghtaling, B. D. Wilts and M. Mayer, *Advanced Materials*, 2018, **30**, 1705322.

35. G. S. Watson, D. W. Green, B. W. Cribb, C. L. Brown, C. R. Meritt, M. J. Tobin, J. Vongsvivut, M. Sun, A.-P. Liang and J. A. Watson, *ACS Applied Materials & Interfaces*, 2017, **9**, 24381-24392.

36. B. Bhushan, *Philosophical Transactions of the Royal Society A: Mathematical, Physical and Engineering Sciences*, 2009, **367**, 1445-1486.

37. M. Eder, S. Amini and P. Fratzl, *Science*, 2018, **362**, 543-547.

38. Z. Guo and W. Liu, *Plant Science*, 2007, **172**, 1103-1112.

39. Y. T. Cheng, D. E. Rodak, C. A. Wong and C. A. Hayden, *Nanotechnology*, 2006, **17**, 1359.

40. A. Marmur, *Langmuir*, 2004, **20**, 3517-3519.

41. L. Gao and T. J. McCarthy, *Langmuir*, 2006, **22**, 2966-2967.

42. R. Fürstner, W. Barthlott, C. Neinhuis and P. Walzel, *Langmuir*, 2005, **21**, 956-961.

43. C. Neinhuis and W. Barthlott, *Annals of Botany*, 1997, **79**, 667-677.

44. X. Gao and L. Jiang, *Nature*, 2004, **432**, 36.

45. D. M. Schroeder and M. S. Love, *Ocean & Coastal Management*, 2004, **47**, 21-48.

46. F. Guo and Z. Guo, *RSC Advances*, 2016, **6**, 36623-36641.

47. G. Ahmed, O. Arjmandi Tash, J. Cook, A. Trybala and V. Starov, *Adv Colloid Interface Sci*, 2017, **249**, 17-36.

48. Y. Kaufman, S.-Y. Chen, H. Mishra, A. M. Schrader, D. W. Lee, S. Das, S. H. Donaldson and J. N. Israelachvili, *The Journal of Physical Chemistry C*, 2017, **121**, 5642-5656.

49. G. Whyman and E. Bormashenko, *Langmuir*, 2011, **27**, 8171-8176.

50. O. Arjmandi-Tash, N. M. Kovalchuk, A. Trybala, I. V. Kuchin and V. Starov, *Langmuir*, 2017, **33**, 4367-4385.

51. N. R. Biswal and S. Paria, *Industrial & Engineering Chemistry Research*, 2012, **51**, 10172-10178.

52. E. A. Vogler, *Advances in Colloid and Interface Science*, 1998, **74**, 69-117.

53. B. Su, Y. Tian and L. Jiang, *Journal of the American Chemical Society*, 2016, **138**, 1727-1748.

54. A. Lafuma and D. Quere, *Nat Mater*, 2003, **2**, 457-460.

55. J. Long, L. Pan, P. Fan, D. Gong, D. Jiang, H. Zhang, L. Li and M. Zhong, *Langmuir*, 2016, **32**, 1065-1072.

56. H.-J. Butt, I. V. Roisman, M. Brinkmann, P. Papadopoulos, D. Vollmer and C. Semprebon, *Current Opinion in Colloid & Interface Science*, 2014, **19**, 343-354.

57. A. K. Gnanappa, D. P. Papageorgiou, E. Gogolides, A. Tserepi, A. G. Papathanasiou and A. G. Boudouvis, *Plasma Processes and Polymers*, 2012, **9**, 304-315.

58. E. Bormashenko, R. Pogreb, G. Whyman and M. Erlich, *Langmuir*, 2007, **23**, 6501-6503.

59. G. McHale, S. Aqil, N. J. Shirtcliffe, M. I. Newton and H. Y. Erbil, *Langmuir*, 2005, **21**, 11053-11060.

60. M. Reyssat, J. M. Yeomans and D. Quéré, *EPL (Europhysics Letters)*, 2008, **81**, 26006.

61. H. Kusumaatmaja, M. L. Blow, A. Dupuis and J. M. Yeomans, *EPL (Europhysics Letters)*, 2008, **81**, 36003.

62. M. Lotfi, M. Nejib and M. Naceur, 2013, DOI: 10.5772/53542.

63. M. Sedighi Moghaddam, M. E. P. Wålinder, P. M. Claesson and A. Swerin, *Langmuir*, 2013, **29**, 12145-12153.

64. D. Campbell, S. M. Carnell and R. J. Eden, *Eye Contact Lens*, 2013, **39**, 254-262.

65. R. Finn, J. McCuan and H. C. Wente, *Journal of Mathematical Fluid Mechanics*, 2011, **14**, 445-453.

66. M. Schleicher, J. Hansmann, B. Elkin, P. J. Kluger, S. Liebscher, A. J. Huber, O. Fritze, C. Schille, M. Muller, K. Schenke-Layland, M. Seifert, H. Walles, H. P. Wendel and U. A. Stock, *Int J Biomater*, 2012, **2012**, 397813.

67. F. J. Higuera, A. Medina and A. Liñán, *Physics of Fluids*, 2008, **20**, 102102.

68. C. W. Extrand and S. I. Moon, *J Colloid Interface Sci*, 2014, **431**, 200-203.

69. Z. Liu, Y. Wang, F. J. Muzzio, G. Callegari and G. Drazer, *Langmuir*, 2017, **33**, 56-65.

70. F. Restagno, C. Poulard, C. Cohen, L. Vagharchakian and L. Leger, *Langmuir*, 2009, **25**, 11188-11196.

71. O. I. del Río, D. Y. Kwok, R. Wu, J. M. Alvarez and A. W. Neumann, *Colloids and Surfaces A: Physicochemical and Engineering Aspects*, 1998, **143**, 197-210.

72. A. F. Stalder, T. Melchior, M. Müller, D. Sage, T. Blu and M. Unser, *Colloids and Surfaces A: Physicochemical and Engineering Aspects*, 2010, **364**, 72-81.

73. A. Mendez-Vilas, A. B. Jodar-Reyes and M. L. Gonzalez-Martin, *Small*, 2009, **5**, 1366-1390.

74. E. Hosono, S. Fujihara, I. Honma and H. Zhou, *Journal of the American Chemical Society*, 2005, **127**, 13458-13459.

75. R. N. Wenzel, *Industrial & Engineering Chemistry*, 1936, **28**, 988-994.

76. S. Wang and L. Jiang, *Advanced Materials*, 2007, **19**, 3423-3424.

77. M. J. Kreder, J. Alvarenga, P. Kim and J. Aizenberg, *Nature Reviews Materials*, 2016, **1**, 15003.

78. C. K. W. Friedli, *Chimie générale pour ingénieur*, Presses polytechniques et universitaires romandes, Lausanne, 2002.

79. Kruss, *Journal*, 1999.

80. K. Tadanaga, J. Morinaga, A. Matsuda and T. Minami, *Chemistry of Materials*, 2000, **12**, 590-592.

81. Y.-C. Sheen, Y.-C. Huang, C.-S. Liao, H.-Y. Chou and F.-C. Chang, *Journal of Polymer Science Part B: Polymer Physics*, 2008, **46**, 1984-1990.

82. M. Manca, A. Cannavale, L. De Marco, A. S. Aricò, R. Cingolani and G. Gigli, *Langmuir*, 2009, **25**, 6357-6362.

83. H. Yang, P. Pi, Z.-Q. Cai, X. Wen, X. Wang, J. Cheng and Z.-r. Yang, *Applied Surface Science*, 2010, **256**, 4095-4102.

84. Q. F. Xu, J. N. Wang and K. D. Sanderson, *ACS Nano*, 2010, **4**, 2201-2209.

85. R. V. Lakshmi, T. Bharathidasan and B. J. Basu, *Applied Surface Science*, 2011, **257**, 10421-10426.

86. B. Xu, Y. Ding, S. Qu and Z. Cai, *Applied Surface Science*, 2015, **356**, 951-957.

87. W. Ma, H. Wu, Y. Higaki, H. Otsuka and A. Takahara, *Chem Commun (Camb)*, 2012, **48**, 6824-6826.

88. S. A. Mahadik, M. S. Kavale, S. K. Mukherjee and A. V. Rao, *Applied Surface Science*, 2010, **257**, 333-339.

89. E. K. Kim, T. Hwang and S. S. Kim, *J Colloid Interface Sci*, 2011, **364**, 561-565.

90. H. Zhang, C. Hou, L. Song, Y. Ma, Z. Ali, J. Gu, B. Zhang, H. Zhang and Q. Zhang, *Chemical Engineering Journal*, 2018, **334**, 598-610.

91. H. N. Tran, Y.-F. Wang, S.-J. You and H.-P. Chao, *Process Safety and Environmental Protection*, 2017, **107**, 168-180.

92. N. Yokoi, K. Manabe, M. Tenjimbayashi and S. Shiratori, *ACS Applied Materials & Interfaces*, 2015, **7**, 4809-4816.

93. M. S. Kavale, D. B. Mahadik, V. G. Parale, P. B. Wagh, S. C. Gupta, A. V. Rao and H. C. Barshilia, *Applied Surface Science*, 2011, **258**, 158-162.

94. L. Xu and J. He, *Langmuir*, 2012, **28**, 7512-7518.

95. S. S. Latthe, C. Terashima, K. Nakata and A. Fujishima, *Molecules*, 2014, **19**, 4256-4283.

96. J. Ryu, K. Kim, J. Park, B. G. Hwang, Y. Ko, H. Kim, J. Han, E. Seo, Y. Park and S. J. Lee, *Scientific Reports*, 2017, **7**, 1981.

97. H. Liu, S. W. Gao, J. S. Cai, C. L. He, J. J. Mao, T. X. Zhu, Z. Chen, J. Y. Huang, K. Meng, K. Q. Zhang, S. S. Al-Deyab and Y. K. Lai, *Materials (Basel)*, 2016, **9**.

98. Q. Wang, X. Yao, H. Liu, D. Quere and L. Jiang, *Proc Natl Acad Sci U S A*, 2015, **112**, 9247-9252.

99. D. Wang, A. Zhao, L. Li, Q. He, H. Guo, H. Sun and Q. Gao, *RSC Advances*, 2015, **5**, 96404-96411.

100. J. Ryu, K. Kim, J. Park, B. G. Hwang, Y. Ko, H. Kim, J. Han, E. Seo, Y. Park and S. J. Lee, *Sci Rep*, 2017, **7**, 1981.

101. H. Y. Gu, Z. Y. Qi, W. Wu, Y. Zeng and L. X. Song, *Express Polymer Letters*, 2014, **8**, 588-595.

102. N. Gupta, M. V. Kavya, Y. R. G. Singh, J. Jyothi and H. C. Barshilia, *Journal of Applied Physics*, 2013, **114**, 164307.

103. J.-H. Oh, T.-J. Ko, M.-W. Moon and C. H. Park, *RSC Advances*, 2017, **7**, 25597-25604.

104. J. Hubert, J. Mertens, T. Dufour, N. Vandencasteele, F. Reniers, P. Viville, R. Lazzaroni, M. Raes and H. Terryn, *Journal of Materials Research*, 2015, **30**, 3177-3191.

105. M. Resnik, R. Zaplotnik, M. Mozetic and A. Vesel, *Materials (Basel)*, 2018, **11**.
106. L. Phan, S. Yoon and M.-W. Moon, *Polymers*, 2017, **9**, 417.
107. M. Cao, D. Guo, C. Yu, K. Li, M. Liu and L. Jiang, *ACS Appl Mater Interfaces*, 2016, **8**, 3615-3623.
108. P. Nguyen-Tri, T. A. Nguyen, P. Carriere and C. Ngo Xuan, *International Journal of Corrosion*, 2018, **2018**, 1-19.
109. C. Yeom and Y. Kim, *Journal of Industrial and Engineering Chemistry*, 2016, **40**, 47-53.
110. F. Wang, S. Arai and M. Endo, *Materials Transactions*, 2004, **45**, 1311-1316.
111. D. Koleva, N. Boshkov, G. Raichevski and L. Veleva, *Transactions of the IMF*, 2013, **83**, 188-193.
112. J. Li, Y. Sun, X. Sun and J. Qiao, *Surface and Coatings Technology*, 2005, **192**, 331-335.
113. M. Shabani-Nooshabadi, S. M. Ghoreishi, Y. Jafari and N. Kashanizadeh, *Journal of Polymer Research*, 2014, **21**.
114. A. A. Farghaly and M. M. Collinson, *Langmuir*, 2016, **32**, 5925-5936.
115. K. M. Cui, M. C. Tria, R. Pernites, C. A. Binag and R. C. Advincula, *ACS Appl Mater Interfaces*, 2011, **3**, 2300-2308.
116. R. Toledano and D. Mandler, *Chemistry of Materials*, 2010, **22**, 3943-3951.
117. C. L. Weaver, J. M. LaRosa, X. Luo and X. T. Cui, *ACS Nano*, 2014, **8**, 1834-1843.
118. F. Fei Fang, H. Jin Choi and J. Joo, *Journal of Nanoscience and Nanotechnology*, 2008, **8**, 1559-1581.
119. Y.-C. Tsai and Y.-H. Hong, *Journal of Solid State Electrochemistry*, 2008, **12**, 1293-1299.
120. P. Gajendran and R. Saraswathi, *Pure and Applied Chemistry*, 2008, **80**, 2377-2395.
121. Q. Chen, L. Zhao, C. Li and G. Shi, *The Journal of Physical Chemistry C*, 2007, **111**, 18392-18396.
122. X. Pang and I. Zhitomirsky, *Surface and Coatings Technology*, 2008, **202**, 3815-3821.
123. X. L. Luo, J. J. Xu, J. L. Wang and H. Y. Chen, *Chem Commun (Camb)*, 2005, DOI: 10.1039/b419197h, 2169-2171.
124. X. Pang and I. Zhitomirsky, *Materials Chemistry and Physics*, 2005, **94**, 245-251.
125. G. Barati Darband, M. Aliofkhazraei, S. Khorsand, S. Sokhanvar and A. Kaboli, *Arabian Journal of Chemistry*, 2018, DOI: 10.1016/j.arabjc.2018.01.013.
126. B. Pijáková, M. Klíma, M. Alberti and V. Buršíková, *Materials Letters*, 2016, **184**, 243-247.
127. R. Jain and R. Pitchumani, *Langmuir*, 2018, **34**, 3159-3169.
128. B. Zhang, Y. Li and B. Hou, *RSC Advances*, 2015, **5**, 100000-100010.
129. E. Vazirinasab, R. Jafari and G. Momen, *Surface and Coatings Technology*, 2018, **341**, 40-56.
130. A. Fihri, E. Bovero, A. Al-Shahrani, A. Al-Ghamdi and G. Alabedi, *Colloids and Surfaces A: Physicochemical and Engineering Aspects*, 2017, **520**, 378-390.
131. J. T. Simpson, S. R. Hunter and T. Aytug, *Rep Prog Phys*, 2015, **78**, 086501.
132. N. Cohen, A. Dotan, H. Dodiuk and S. Kenig, *Materials and Manufacturing Processes*, 2015, **31**, 1143-1155.
133. P. F. Rios, H. Dodiuk, S. Kenig, S. McCarthy and A. Dotan, *Journal of Adhesion Science and Technology*, 2007, **21**, 399-408.

134. W. Zeng, J. Chen, H. Yang, L. Deng, G. Liao and Z. Xu, *Surface and Coatings Technology*, 2017, **309**, 1045-1051.

135. X. Ding, S. Zhou, G. Gu and L. Wu, *Journal of Materials Chemistry*, 2011, **21**, 6161.

136. P. Cataldi, I. S. Bayer, R. Cingolani, S. Marras, R. Chellali and A. Athanassiou, *Scientific Reports*, 2016, **6**, 27984.

137. I. Bayer, *Coatings*, 2017, **7**, 12.

138. X.-T. Zhang, O. Sato, M. Taguchi, Y. Einaga, T. Murakami and A. Fujishima, *Chemistry of Materials*, 2005, **17**, 696-700.

139. L. Li, Y. Bai, L. Li, S. Wang and T. Zhang, *Advanced Materials*, 2017, **29**, 1702517.

140. Z. H. Zhang, H. J. Wang, Y. H. Liang, X. J. Li, L. Q. Ren, Z. Q. Cui and C. Luo, *Sci Rep*, 2018, **8**, 3869.

141. M. Wahl, *Marine Ecology Progress Series*, 1989, **58**, 175-189.

142. T. Muthukumar, A. Aravinthan, K. Lakshmi, R. Venkatesan, L. Vedaprakash and M. Doble, *International Biodeterioration & Biodegradation*, 2011, **65**, 276-284.

143. M. Lagerstrom, J. Strand, B. Eklund and E. Ytreberg, *Environ Pollut*, 2017, **220**, 1333-1341.

144. A. Kotrikla, *J Environ Manage*, 2009, **90 Suppl 1**, S77-85.

145. Y. Dang, M. Quan, C.-M. Xing, Y.-B. Wang and Y.-K. Gong, *Journal of Materials Chemistry B*, 2015, **3**, 2350-2361.

146. M. S. Selim, M. A. Shenashen, S. A. El-Safty, S. A. Higazy, M. M. Selim, H. Isago and A. Elmarakbi, *Progress in Materials Science*, 2017, **87**, 1-32.

147. M. Cloutier, D. Mantovani and F. Rosei, *Trends Biotechnol*, 2015, **33**, 637-652.

148. S. Heinonen, J. P. Nikkanen, J. Laakso, M. Raulio, O. Priha and E. Levänen, *IOP Conference Series: Materials Science and Engineering*, 2013, **47**, 012064.

149. *Coatings*, 2018, **8**, 101.

150. W. He, Y. Zhang, J. Li, Y. Gao, F. Luo, H. Tan, K. Wang and Q. Fu, *Scientific Reports*, 2016, **6**, 32140.

151. H. Sojoudi, M. Wang, N. D. Boscher, G. H. McKinley and K. K. Gleason, *Soft Matter*, 2016, **12**, 1938-1963.

152. S. Ozbay, C. Yuceel and H. Y. Erbil, *ACS Appl Mater Interfaces*, 2015, **7**, 22067-22077.

153. R. C. Little, R. J. Hansen, D. L. Hunston, O.-K. Kim, R. L. Patterson and R. Y. Ting, *Industrial & Engineering Chemistry Fundamentals*, 1975, **14**, 283-296.

154. M. N. Kavalenka, F. Vüllers, S. Lischker, C. Zeiger, A. Hopf, M. Röhrig, B. E. Rapp, M. Worgull and H. Hölscher, *ACS Applied Materials & Interfaces*, 2015, **7**, 10651-10655.

155. K. Liu, Y. Tian and L. Jiang, *Progress in Materials Science*, 2013, **58**, 503-564.

156. M. R. Maghami, H. Hizam, C. Gomes, M. A. Radzi, M. I. Rezadad and S. Hajighorbani, *Renewable and Sustainable Energy Reviews*, 2016, **59**, 1307-1316.

157. A. Massi Pavan, A. Mellit and D. De Pieri, *Solar Energy*, 2011, **85**, 1128-1136.

158. M. S. El-Shobokshy and F. M. Hussein, *Solar Energy*, 1993, **51**, 505-511.

159. T. Sarver, A. Al-Qaraghuli and L. L. Kazmerski, *Renewable and Sustainable Energy Reviews*, 2013, **22**, 698-733.

160. M. S. Ngan and C. W. Tan, 2011, DOI: 10.1109/iapec.2011.5779863, 22-27.

161. M. Sheraz and M. A. Abido, 2012, DOI: 10.1109/PECon.2012.6450241, 378-383.
162. R. Blossey, *Nature Materials*, 2003, **2**, 301.
163. G. Gu, H. Dang, Z. Zhang and Z. Wu, *Applied Physics A*, 2006, **83**, 131-132.
164. I. P. Parkin and R. G. Palgrave, *Journal of Materials Chemistry*, 2005, **15**, 1689-1695.
165. H. J. Gwon, Y. Park, C. W. Moon, S. Nahm, S.-J. Yoon, S. Y. Kim and H. W. Jang, *Nano Research*, 2014, **7**, 670-678.
166. Y.-B. Park, H. Im, M. Im and Y.-K. Choi, *Journal of Materials Chemistry*, 2011, **21**, 633-636.
167. Y.-Y. Quan and L.-Z. Zhang, *Solar Energy Materials and Solar Cells*, 2017, **160**, 382-389.
168. J. Liu, Z. A. Janjua, M. Roe, F. Xu, B. Turnbull, K.-S. Choi and X. Hou, *Nanomaterials (Basel, Switzerland)*, 2016, **6**, 232.
169. X. Liu and J. He, *Langmuir*, 2009, **25**, 11822-11826.
170. S. Sutha, S. Suresh, B. Raj and K. R. Ravi, *Solar Energy Materials and Solar Cells*, 2017, **165**, 128-137.
171. A. C. Power, A. Barrett, J. Abubakar, L. J. Suarez, L. Ryan, D. Wencel, T. Sullivan and F. Regan, *Advanced Engineering Materials*, 2016, **18**, 76-82.
172. D. Schondelmaier, S. Cramm, R. Klingeler, J. Morenzin, C. Zilkens and W. Eberhardt, *Langmuir*, 2002, **18**, 6242-6245.
173. Y. Xiu, F. Xiao, D. W. Hess and C. P. Wong, *Thin Solid Films*, 2009, **517**, 1610-1615.
174. Y. Li, W. Cai, B. Cao, G. Duan, F. Sun, C. Li and L. Jia, *Nanotechnology*, 2006, **17**, 238-243.
175. J.-D. Brassard, D. K. Sarkar and J. Perron, *Applied Sciences*, 2012, **2**, 453-464.
176. H. Zhou, H. Wang, H. Niu, A. Gestos, X. Wang and T. Lin, *Adv Mater*, 2012, **24**, 2409-2412.
177. N. Saleema, D. K. Sarkar, D. Gallant, R. W. Paynter and X. G. Chen, *ACS Applied Materials & Interfaces*, 2011, **3**, 4775-4781.
178. S. Liu, X. Liu, S. S. Latthe, L. Gao, S. An, S. S. Yoon, B. Liu and R. Xing, *Applied Surface Science*, 2015, **351**, 897-903.
179. T. M. Mayer, M. P. de Boer, N. D. Shinn, P. J. Clews and T. A. Michalske, *Journal of Vacuum Science & Technology B: Microelectronics and Nanometer Structures*, 2000, **18**, 2433.
180. D. Ambrożewicz, F. Ciesielczyk, M. Nowacka, J. Karasiewicz, A. Piasecki, H. Maciejewski and T. Jesionowski, *Journal of Nanomaterials*, 2013, **2013**, 1-13.
181. H. Ennaceri, H. El Alami, H. Brik, O. Mokssit and A. Khaldoun, 2014, DOI: 10.1109/iccmrea.2014.6843785, 1-4.
182. Dricus, Solar panel nano coatings, https://sinovoltaics.com/technology/solar-panel-nano-coatings-use-or-not/).
183. V. A. Lifton, S. Simon and R. E. Frahm, *Bell Labs Technical Journal*, 2005, **10**, 81-85.
184. W. Li, X. Wang, Z. Chen, M. Waje and Yan, *Langmuir*, 2005, **21**, 9386-9389.
185. X. Zhang, F. Shi, J. Niu, Y. Jiang and Z. Wang, *Journal of Materials Chemistry*, 2008, **18**, 621-633.
186. M. Ma, R. M. Hill, J. L. Lowery, S. V. Fridrikh and G. C. Rutledge, *Langmuir*, 2005, **21**, 5549-5554.
187. M. Ma, Y. Mao, M. Gupta, K. K. Gleason and G. C. Rutledge, *Macromolecules*, 2005, **38**, 9742-9748.
188. Q. T. Truong and N. Pomerantz, 2018, DOI: 10.1016/b978-0-08-101212-3.00016-2, 473-531.

189. B. N. Sahoo, N. S. K. Gunda, S. Nanda, J. A. Kozinski and S. K. Mitra, *ACS Sustainable Chemistry & Engineering*, 2017, **5**, 6716-6726.

190. B. N. Sahoo, S. Nanda, J. A. Kozinski and S. K. Mitra, *RSC Advances*, 2017, **7**, 15027-15040.

191. N. M. Bedford and A. J. Steckl, *ACS Applied Materials & Interfaces*, 2010, **2**, 2448-2455.

192. M. E. Yazdanshenas and M. Shateri-Khalilabad, *Industrial & Engineering Chemistry Research*, 2013, **52**, 12846-12854.

193. C.-H. Xue, Y.-R. Li, P. Zhang, J.-Z. Ma and S.-T. Jia, *ACS Applied Materials & Interfaces*, 2014, **6**, 10153-10161.

194. C.-H. Xue, X. Bai and S.-T. Jia, *Scientific Reports*, 2016, **6**, 27262.

195. I. Das and G. De, *Scientific Reports*, 2015, **5**, 18503.

196. L. Wang, X. Zhang, B. Li, P. Sun, J. Yang, H. Xu and Y. Liu, *ACS Applied Materials & Interfaces*, 2011, **3**, 1277-1281.

197. K. Ellinas, D. Kefallinou, K. Stamatakis, E. Gogolides and A. Tserepi, *ACS Applied Materials & Interfaces*, 2017, **9**, 39781-39789.

198. B. J. Privett, J. Youn, S. A. Hong, J. Lee, J. Han, J. H. Shin and M. H. Schoenfisch, *Langmuir*, 2011, **27**, 9597-9601.

199. C. Zhou, Z. Chen, H. Yang, K. Hou, X. Zeng, Y. Zheng and J. Cheng, *ACS Applied Materials & Interfaces*, 2017, **9**, 9184-9194.

200. X. Zhou, Z. Zhang, X. Xu, F. Guo, X. Zhu, X. Men and B. Ge, *ACS Applied Materials & Interfaces*, 2013, **5**, 7208-7214.

201. Q.-Y. Cheng, X.-P. An, Y.-D. Li, C.-L. Huang and J.-B. Zeng, *ACS Sustainable Chemistry & Engineering*, 2017, **5**, 11440-11450.

202. C. Zhou, X. Gong, W. Zhang, J. Han, R. Guo and A. Zhu, *Water Environment Research*, 2017, **89**, 817-826.

203. A. Tripathy, A. Kumar, S. Sreedharan, G. Muralidharan, A. Pramanik, D. Nandi and P. Sen, *ACS Biomaterials Science & Engineering*, 2018, **4**, 2213-2223.

204. M. Li, L. Gao, C. Schlaich, J. Zhang, I. S. Donskyi, G. Yu, W. Li, Z. Tu, J. Rolff, T. Schwerdtle, R. Haag and N. Ma, *ACS Applied Materials & Interfaces*, 2017, **9**, 35411-35418.

205. M. J. Kratochvil, Y. Tal-Gan, T. Yang, H. E. Blackwell and D. M. Lynn, *ACS Biomaterials Science & Engineering*, 2015, **1**, 1039-1049.

206. B. Liang, G. Zhang, Z. Zhong, Y. Huang and Z. Su, *Langmuir*, 2018, DOI: 10.1021/acs.langmuir.8b01009.

207. Y. Lin, H. Chen, G. Wang and A. Liu, *Coatings*, 2018, **8**, 208.

208. C.-H. Xue, X.-J. Guo, J.-Z. Ma and S.-T. Jia, *ACS Applied Materials & Interfaces*, 2015, **7**, 8251-8259.

209. A. Nakajima, K. Hashimoto, T. Watanabe, K. Takai, G. Yamauchi and A. Fujishima, *Langmuir*, 2000, **16**, 7044-7047.

210. J. X. H. Wong and H.-Z. Yu, *Journal of Chemical Education*, 2013, **90**, 1203-1206.

211. L. Xiao, W. Zeng, G. Liao, C. Yi and Z. Xu, *ACS Applied Nano Materials*, 2018, **1**, 1204-1211.

212. Q. F. Xu, Y. Liu, F.-J. Lin, B. Mondal and A. M. Lyons, *ACS Applied Materials & Interfaces*, 2013, **5**, 8915-8924.

213. A. Andaloro, E. S. Mazzucchelli, A. Lucchini and M. P. Pedeferri, *Journal of Facade Design and Engineering*, 2017, **4**, 115-129.

214. D. S. Facio and M. J. Mosquera, *ACS Applied Materials & Interfaces*, 2013, **5**, 7517-7526.

215. X.-D. Xu, X. Chen, B. Yu, Z.-Z. Guan, H.-L. Cong, Q.-H. Peng and M.-M. Jiao, *Integrated Ferroelectrics*, 2016, **170**, 92-99.

216. K.-i. Katsumata, S. Okazaki, C. E. J. Cordonier, T. Shichi, T. Sasaki and A. Fujishima, *ACS Applied Materials & Interfaces*, 2010, **2**, 1236-1241.

217. J.-G. Lee, S. An, T.-G. Kim, M.-W. Kim, H.-S. Jo, M. T. Swihart, A. L. Yarin and S. S. Yoon, *ACS Applied Materials & Interfaces*, 2017, **9**, 35325-35332.

218. M. Faustini, L. Nicole, C. Boissière, P. Innocenzi, C. Sanchez and D. Grosso, *Chemistry of Materials*, 2010, **22**, 4406-4413.

219. D. Ebert and B. Bhushan, *Langmuir*, 2012, **28**, 11391-11399.

220. F.-F. Chen, Y.-J. Zhu, Z.-C. Xiong, T.-W. Sun and Y.-Q. Shen, *ACS Applied Materials & Interfaces*, 2016, **8**, 34715-34724.

221. J. Zhang, W. Lin, C. Zhu, J. Lv, W. Zhang and J. Feng, *Langmuir*, 2018, **34**, 5600-5605.

222. D. Helmer, N. Keller, F. Kotz, F. Stolz, C. Greiner, T. M. Nargang, K. Sachsenheimer and B. E. Rapp, *Scientific Reports*, 2017, **7**, 15078.

223. G. Fortin, *SAE Technical Paper* , 2017, 19.

224. A. M. A. Mohamed, A. M. Abdullah and N. A. Younan, *Arabian Journal of Chemistry*, 2015, **8**, 749-765.

225. P. M. Rao a, Ramamurthy P, presented in part at the *Energy Procedia*, 2014.

226. H. Mohammad Rez Maghami, ChandimaGomes, Mohd AmranRadzi, Mohammad Ismael Rezadad, ShahroozHajighorbani, *Renewable and Sustainable Energy Reviews*, 2017, **59**, 1307-1316.

227. A. W. Bunyan H, Alnaser M. , *Smart Grid and Renewable Energy*, 2016, **7**, 190-196.

228. K. A. Ameri A, P Zarafshan, S Kouravan, M. Khashehchi, presented in part at the *proceeding of 3rd ICESE*, 2016.

229. H. K. Abbas Z, P. Hameed , F. Bhayod , *Noble Int J. Sci Res*, 2017, 73-79.

230. B. R. Paudyal, S. R. Shakya, D. P. Paudyal and D. Das Mulmi, *Renewables: Wind, Water, and Solar*, 2017, **4**, 5.

231. Y. Sukamongkol, *J. Sust. Ener. Environ*, 2015, 33-36.

232. J. Y. Bhushan B, *Progress in Materials Science*, 2011, **56**.

234. A. B. Gurav, S. S. Latthe, R. S. Vhatkar, J.-G. Lee, D.-Y. Kim, J.-J. Park and S. S. Yoon, *Ceramics International*, 2014, **40**, 7151-7160.

235. C.-A. Lin, M.-L. Tsai, W.-R. Wei, K.-Y. Lai and J.-H. He, *ACS Nano*, 2016, **10**, 549-555.

- F. Beshkar, H. Khojasteh, M. Salavati-Niasari. *Materials* 2017, **10**, 697; doi: 10.3390/ma10070697

- H. Najafian, F. Manteghi, F. Beshkar, M. Salavati-Niasaric. *J. Hazard. Mater.* 2019, **361**, 210–220.
- H. Najafian, F. Manteghi, F. Beshkar, M. Salavati-Niasari. *Sep. Purif. Technol.,* 2018, **195**, 30–36.
- H. Najafian, F. Manteghi, F. Beshkar, M. Salavati-Niasaric. *Sep. Purif. Technol.*, 2019, **209**, 6–17.
- E. Esmaeili, M. Salavati-Niasaria, F. Mohandes, F. Davar, H. Seyghalkar. *Chem. Eng. J.* 2011, **170**, 278-285.
- S. M. Hosseinpour-Mashkani, F. Mohandes, M. Salavati-Niasari, K.Venkateswara-Rao. *Mater. Res. Bull.* 2012, **47**, 3148-3159.
- M. Salavati-Niasari, F. Davar, M. Mazaheri. *J. Alloy. Compd.*, 2009, **470**, 502-506.
- M. Salavati-Niasari. *Chem. Lett.*, 2005, **34,** 1444-1445.
- M. Salavati-Niasari, M. Dadkhah, F. Davar. *Inorganica Chimica Acta* 2009, **362**, 3969-3974.
- G. Kianpour, M. Salavati-Niasari, H. Emadi. *Ultrason. Sonochem.* 2013, **20**, 418-424.
- F. Mohandes, M. Salavati-Niasari. *Ultrason. Sonochem.* 2013, **20**, 354-365.

Table 1. Theories available to measure the solid surface energy[79]

Theory	Definition	Surface type
Zisman (one component model)	Contact angle is of 0°. The solid surface is totally wetted by the liquid	Adequate: Non-polar surfaces Non-adequate: polymeric, glass, ceramics and metallic surfaces.
Owens/Wendt or harmonic mean method (two component model)	Surface have both dispersive and polar components	Adequate: surfaces with low surface charge and moderately polar
Fowkes (two component model)	Surface energy has dispersive and a polar component. The measurement of the contact angle starts with a dispersive liquid (diiodomethane) and then a liquid having both a dispersive and polar component (water).	Adequate: adhesive and coating
Van Oss (three component model)	The surface energy has three components (dispersive, acid and base)	Adequate: inorganic surfaces, organometallic surface, ionic surfaces.

1232 **Table 2**. Main applications of superhydrophobic coatings and theirs required properties

Applications	Products	Main requirements	References
Textile industry	Self-cleaning textiles	Mechanical and detergent resistance, flexible	191-195
	Antibacterial textiles	High biological activity, low human toxic, flexible	193, 196-198
	Filtration membranes	High efficient, recyclability, flexible	199-202
Coating industry	Antibacterial coatings	High biological activity and weather resistance	203-205
	Anti-icing coatings	Low surface energy, low toxic	24, 206, 207
	Antifouling coatings	Non-toxic metallic nanoparticles, high durability	28, 208
Construction	Self-cleaning glasses	Good adhesion with glasses, high weather and mechanical resistance, transparent	209-211
	Photo catalysis walls	High sensibility to UV, high transformation efficient	212, 213
			212, 213
	Superhydrophobic stones and building materials	Resistance to weathering	214
		High CA, high weather resistance, good durability	
Automobile	Self-cleaning paints	High CA, high weather resistance	23, 215
	Self-cleaning glasses	Good adhesion with glasses, high weather and mechanical resistance, transparent	23, 215-217
Energy	Transparent coatings for solar cells	High weather and mechanical resistance, transparent, water resistance	218, 219
	Batteries	High chemical resistance	220
Aerospace	Reflective paints	High mechanical and thermal resistance	221, 222
	Anti-icing paints	Low surface energy, low toxic	24, 223
	Self-cleaning paint	High CA, excellent mechanical and thermal resistance	224

1233

1234

1235 **Table 3:** Effect of dust on solar panel's efficiency

1236

Location	Panel condition	Specifications	Results	Ref.
University of Malaga, Spain	One cell was cleaned daily, another contained dust and only been cleaned by rain.	Dry summer to rainfall. 30° tilt angle	Mean daily loss observed 4.4%. Average monthly loss 2%. The losses values observed minimum at solar noon, then increased to the maximum value (≈75°), and then decreased.	225
Albuquerque, USA	Two panels	Spraying the surface of photovoltaic cells can recover 95% of the reflectance losses	The mobile system was used for cleaning	226
Bangalore, India	One was indoor setup with or without dust. Another was outdoor system with and without dust.	Tilt angle of 13° southwards.	Current drop rate with respect to clean panel was more in indoor system. 5-6% drop in power loss observed because of dust density of 1.40 g/m^2 compared to maximum possible power output with cleaned photovoltaic system in outdoor unit. Due to dust density of 7.15 g/m^2. Power loss measured 45-55% of the maximum power output compared to cleaned panel in indoor system.	227
Kuwait city, Kuwait	Two panels were placed in open environment. One panel was cleaned daily and second was cleaned monthly. Impurity accumulation increased in the months of April, May, October and December by 90%, 72%, 27% and 11.26% respectively, and decreased in the months	Tilt angle of 30˚ from ground, facing south. Duration: one year.	The reduction on the panel efficiency was observed in the months of April, May, October and December by 15.07%, 13.74%, 10.68% and 8.74%, respectively compared to clean panel.	228

	of November and June by 63% and 61.5% respectively.			
Pakdasht County, Tehran	Three solar panels were used with 5 g, 10 g, 15 g dust loads.	In this sun simulator, LED lamps were used for creating artificial sunlight; polycarbonate plate and air fan were used to create natural dust deposition.	Maximum amount of reduction in voltage was 8.03% by 15 g dusted panel and minimum amount of reduction was 3.85% by 5 g dusted panel. Vmax loss by 15 g dusted panel was 13.33% Vmax loss by 5 g dusted panel was 6.66% Short circuit current loss noticed was 45.30% by 15 g dusted panel and 26.17% by 5 g dusted panel. Imax loss by 15 g dusted panel was 44.41% Imax loss by 5 g dusted panel was 25.10% Power loss of 51.82% by 15 g dusted panel and 30.10% by 5 g dusted panel.	[229]
Bahawalpur, Pakistan	Two panels were cleaned regularly, and two remained accumulated by dust	The tilt angle of 28° in southward direction for three months of June, July and August. The dust density deposited in the months of June was 0.786 mg/cm^2, July was 0.681 mg/cm^2, and August was 0.601 mg/cm^2	Total output losses occurred were 22%, 15.5%, 10.2%, respectively for June, July and August. 3% overall average efficiency was lost due to dust deposition.	[230]
Kathmandu valley, Nepal	Among two panels, one was cleaned daily, and one was not.	Tilt angle of 27°. Time period: 13 August 2015 to 10 January 2016. Dust deposition density ranged from 0.1047 to	Power reduction was 29.76% with transmittance loss of 2.52% on first day and increased to 69.06% on the last day at 750 nm.	[231]

		9.6711 g/m^2.		
Bhopal, India	Two 36W panels used for 1 year.	The minimum and maximum solar intensity was 210 W/m^2 and 985 W/m^2, respectively	The reduction in power was 92% and reduction in efficiency observed was 89%.	[232]
Bangkok, Thailand	Two glass sheets and two 40W photovoltaic cells were mounted on top of building. One panel and glass pair cleaned daily, and one pair was left uncleaned for 30 days	15° facing to the south.	Transmittance of clean sheet was 90% and uncleaned sheet reduced from 89.8% to 74.9%. The differences between the values of generated power by the clean and uncleaned modules were0.03, 0.07 and 0.11 MJ for 7, 15 and 30 days of exposure, respectively. The conversion efficiencies of the clean photovoltaic module were between 4.78 % and 4.92% and the decrement of the uncleaned module efficiencies was from 4.78% to 4.07%.	[233]

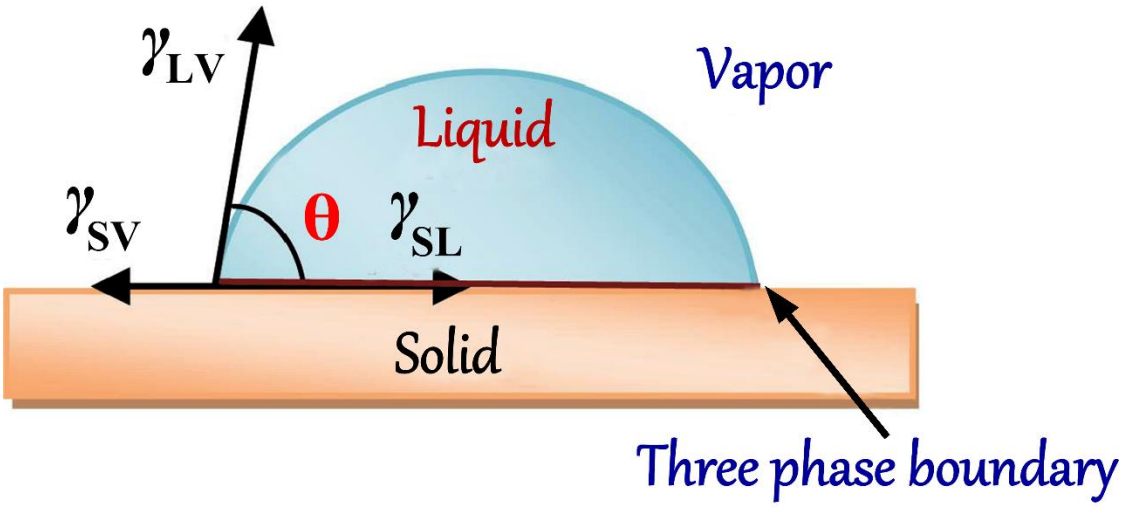

Figure 1. Forces acting at the three phases contact line of a liquid on a solid surface. Reproduced with permission[33]

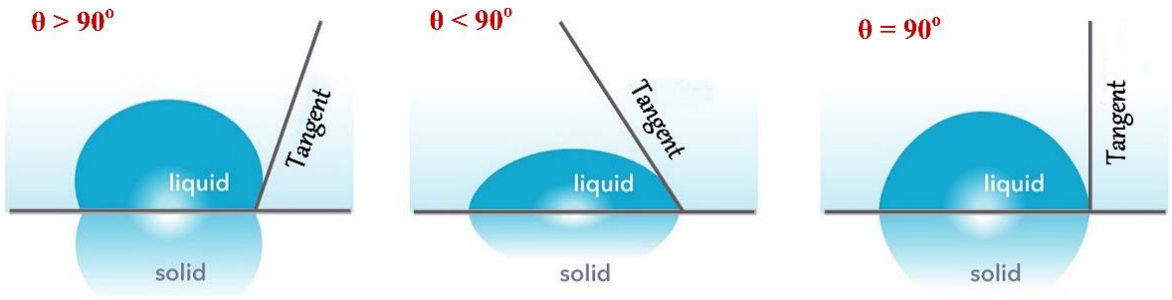

Figure 2. Different wetting surfaces of a liquid drop on a smooth solid surface from the Young's equation of its radius).[59-61]

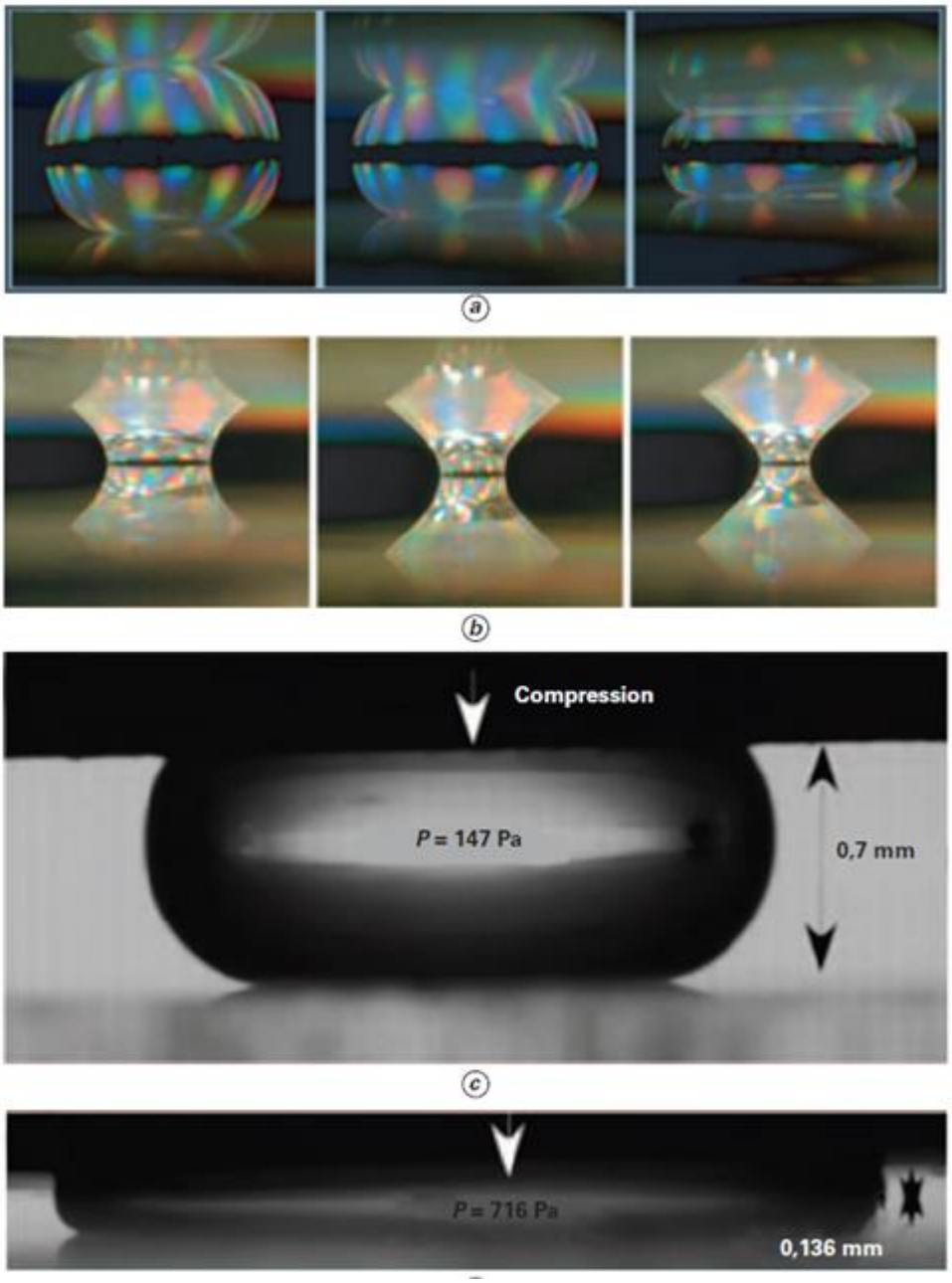

Figure 3. (a) Photograph of a drop of water compressed between two superhydrophobic plates, **(b)** during the separation of the surfaces after transition of wetting,[43] **(c)–(d)** extreme compression of a drop of water against a PMMA superomniphobic surface. Reproduced with permission[54-56]

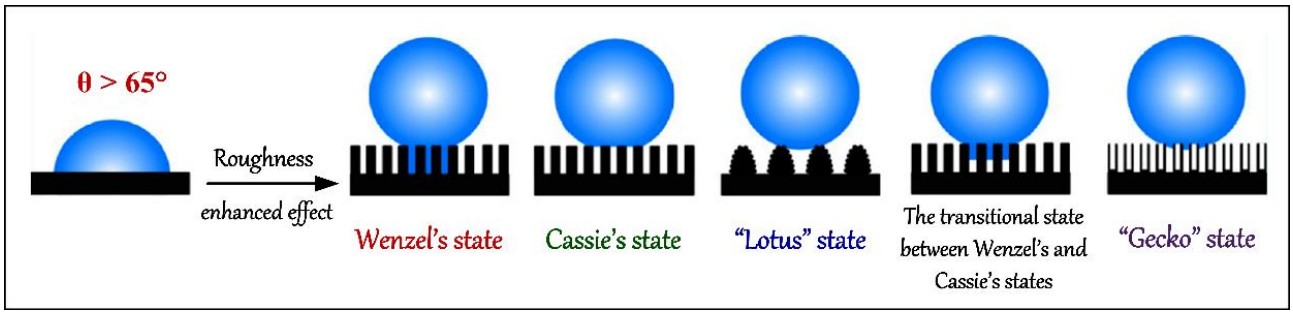

Figure 4. Different states of a water droplet on a solid surface.

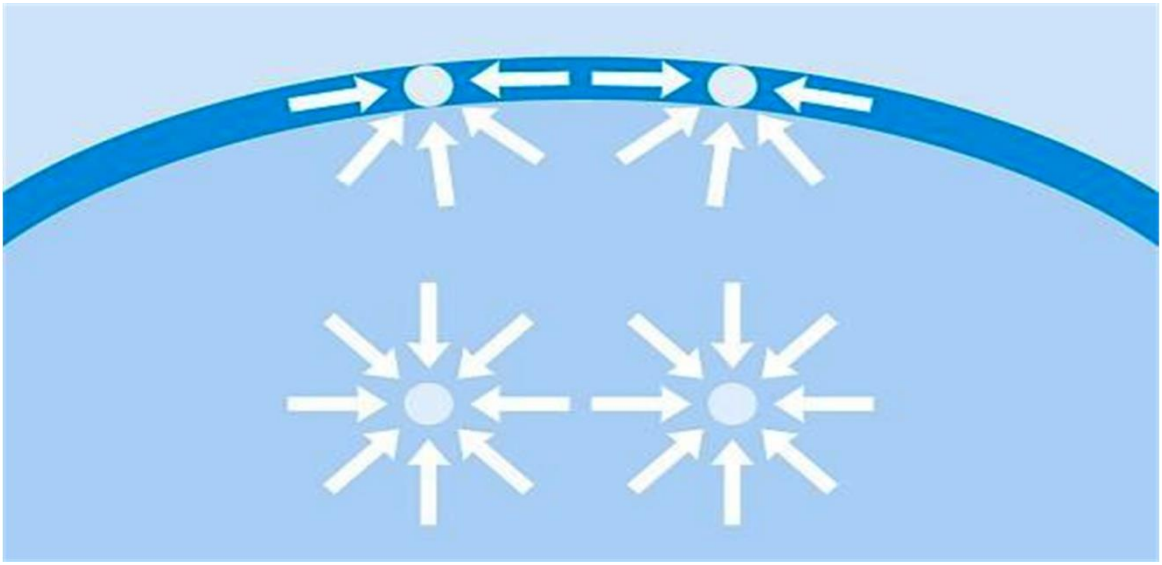

Figure 5. Schematic illustration of surface tension of at a liquid-solid interface due to the unbalanced forces of liquid molecules.

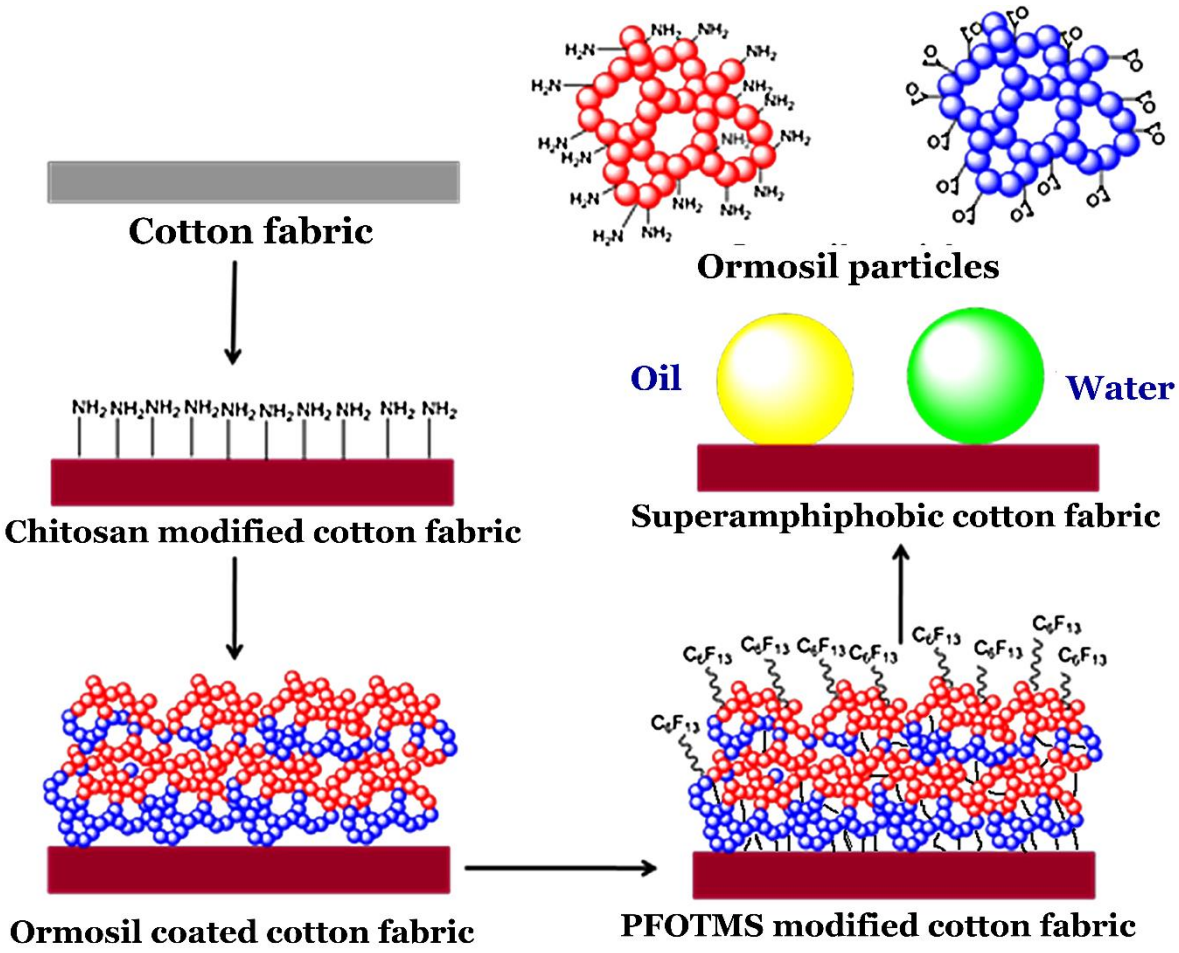

Figure 6. Schematic diagram of the fabrication process for superamphiphobic cotton fabrics. Reproduced with permission[86]

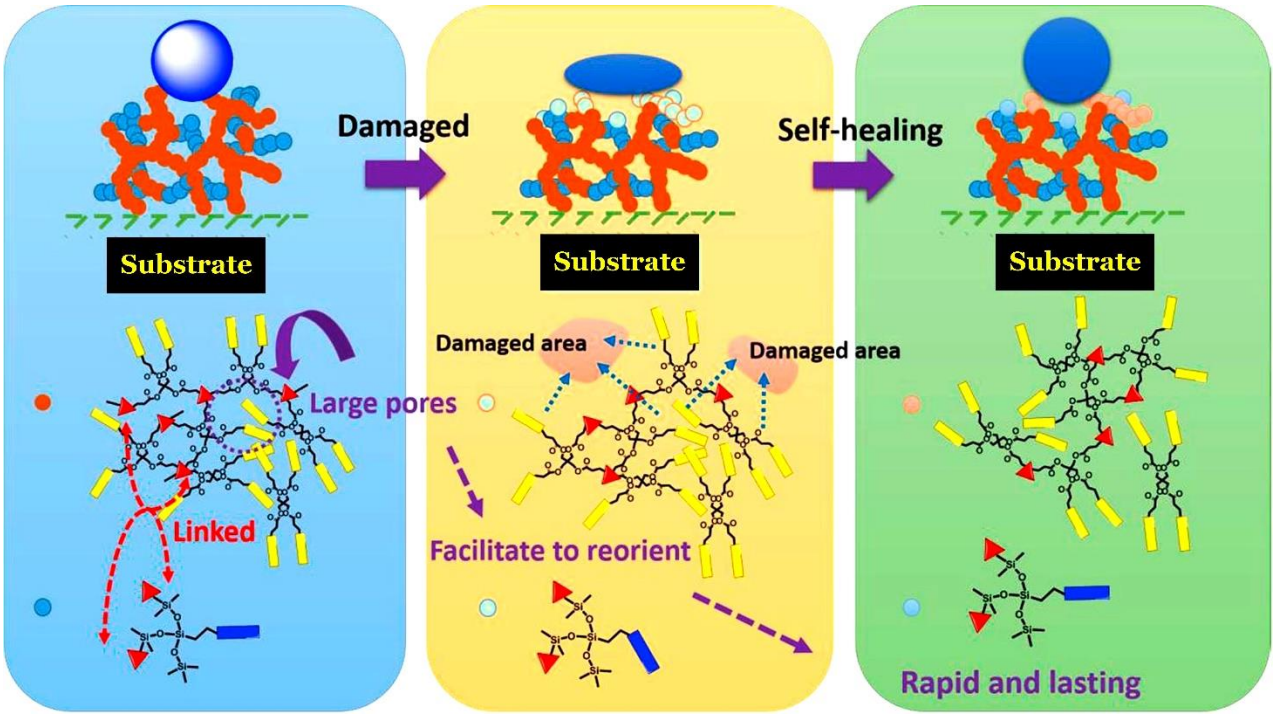

1312 **Figure 7.** Schematic illustration of the rapid, lasting self-healing mechanism for the T-FAS/FOTS

1313 nanocoating layer during damage and self-healing treatment. Reproduced with permission[90]

1314

1315

1316

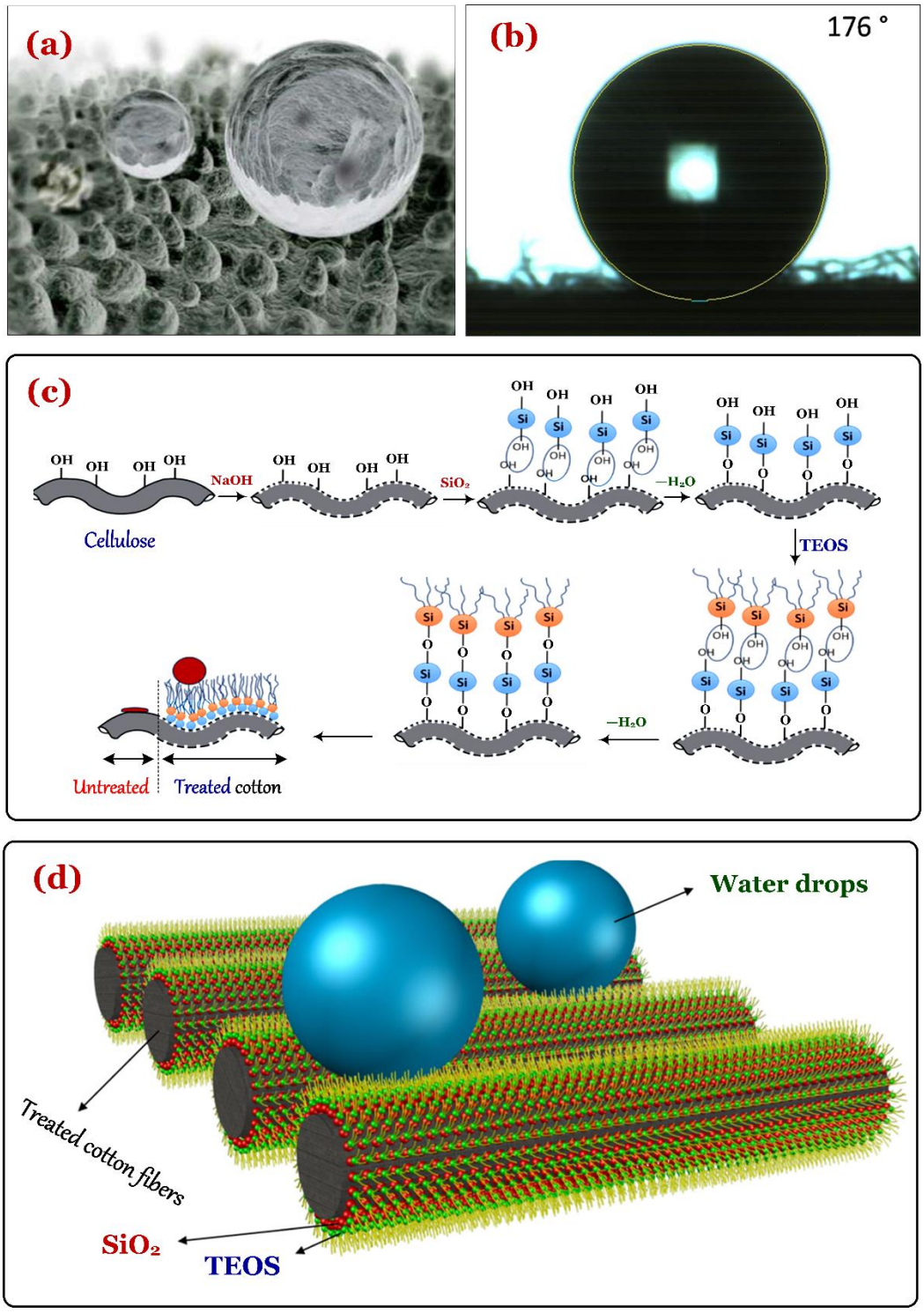

1317 **Figure 8. (a)** Double architectures of lotus leave, **(b)** water drops on a superhydrophobic cotton, **(c)**

1318 chemical etching of cotton fibers, and **(d)** schematic illustration of treated cotton fibers.

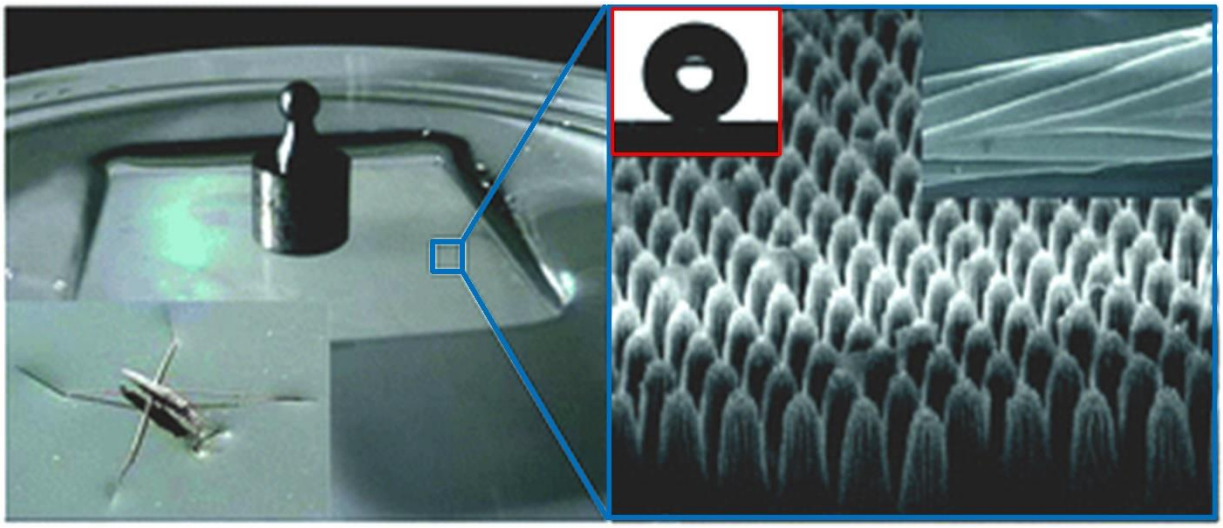

Figure 9. Inspiration of the seta arrays on the legs of water spiders by polymethyl methacrylate (PMMA) substrate using polystyrene (PS) sphere colloidal lithography, followed by oxygen plasma ablation. Reproduced with permission[99]

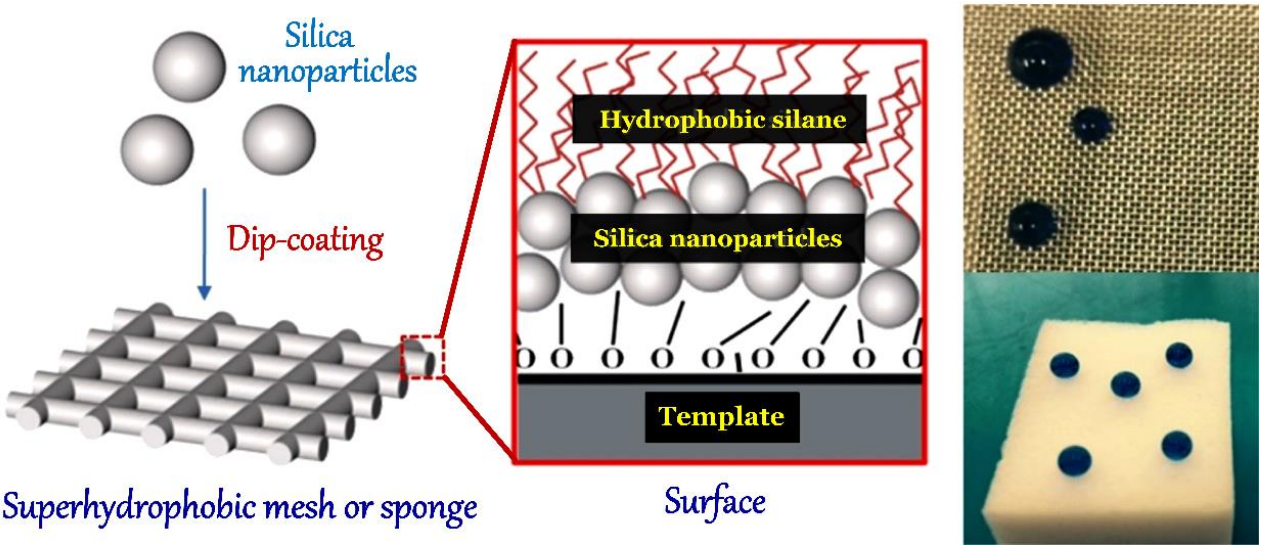

Figure 10. Superhydrophobic coatings from nano-silica and HDTMS, treated mesh and sponge for separation of oil/water mixtures. Reproduced with permission[109]

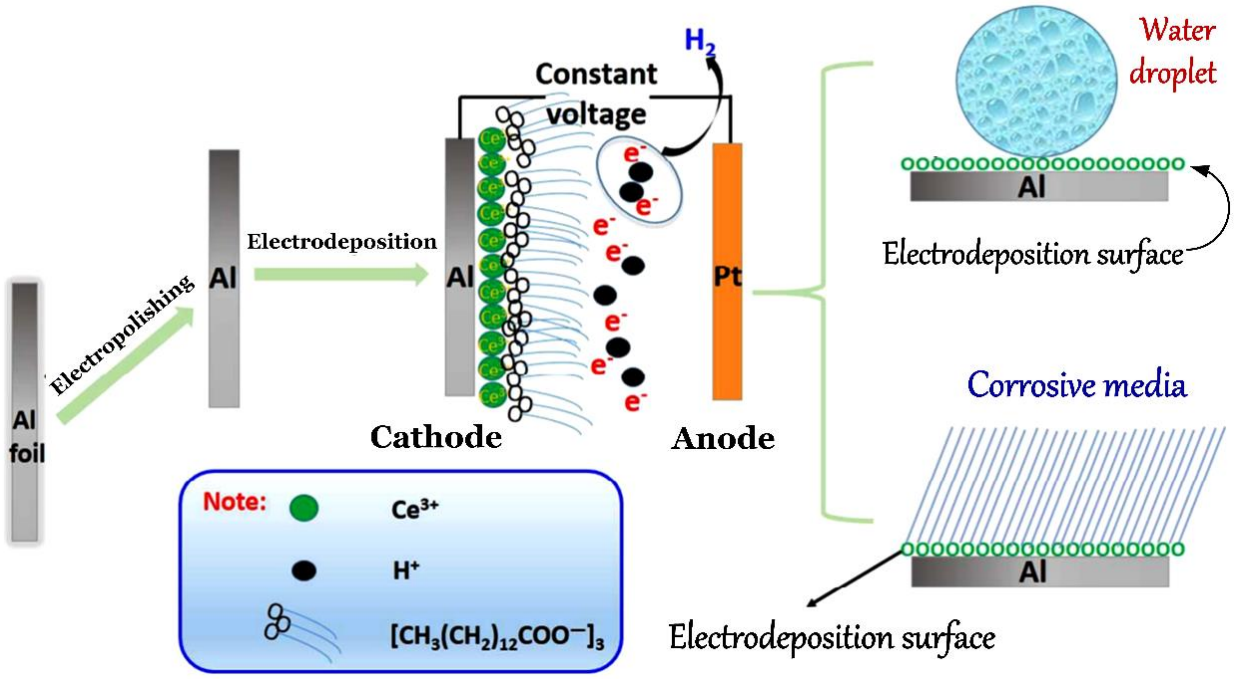

1340 **Figure 11**. Superhydrophobic coatings on Al substrate prepared by electrodeposition. Reproduced with

1341 permission[128]

1342

1343

1344

1345

1346

1347

1348

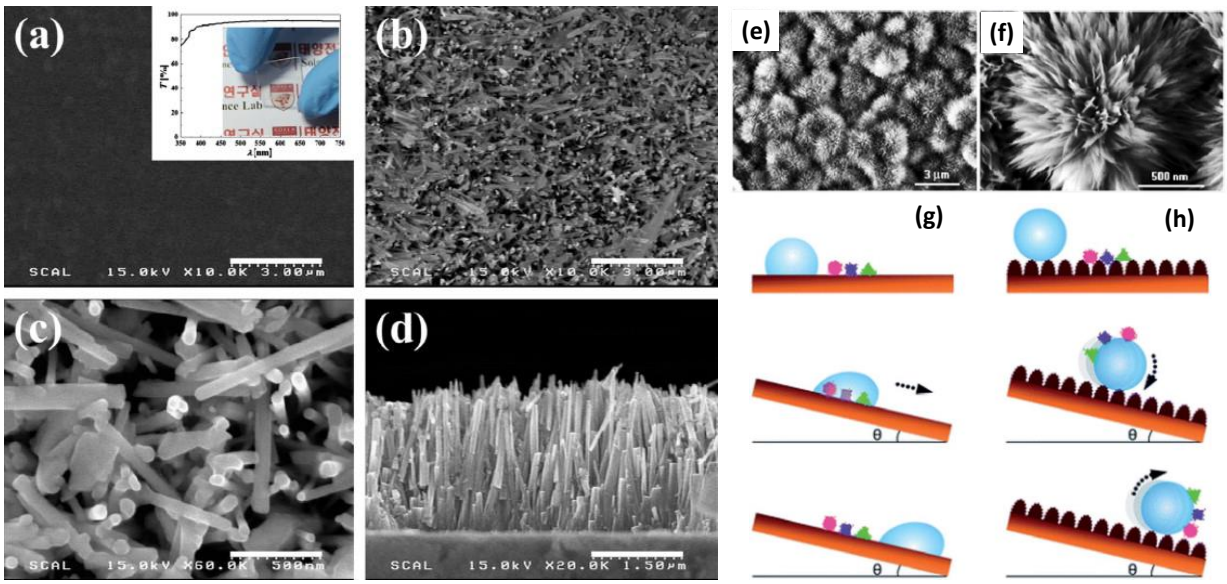

Figure 12. SEM images of **(a)** ZnO seed surface and ZnO nano-rod surface at **(b)** low (3 um) and **(c)** high (500 nm) magnifications and the cross-section SEM image of ZnO nano-rod film; **(e)** low and **(f)** high magnification SEM images of the boehmite film on the aluminum foil prepared using the solution-phase synthesis method; and **(g)** sliding process of the water droplet on the non-hydrophobic and **(h)** superhydrophobic coatings.[95, 234]

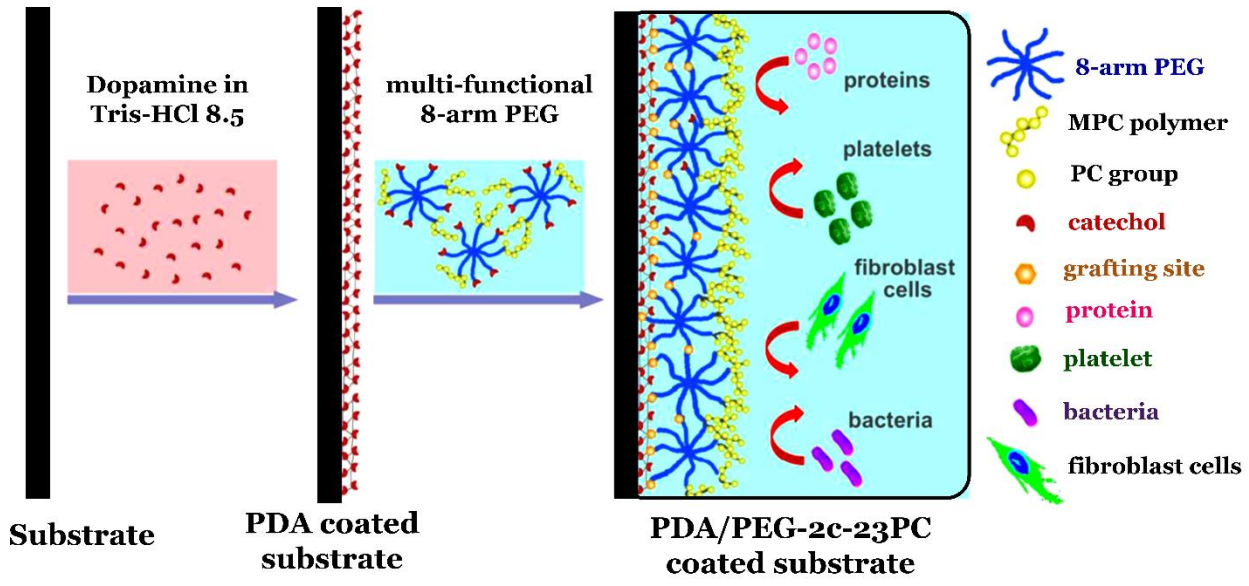

Figure 13. Schematic illustration of a biocompatible and antifouling coating. Reproduced with permission.[145]

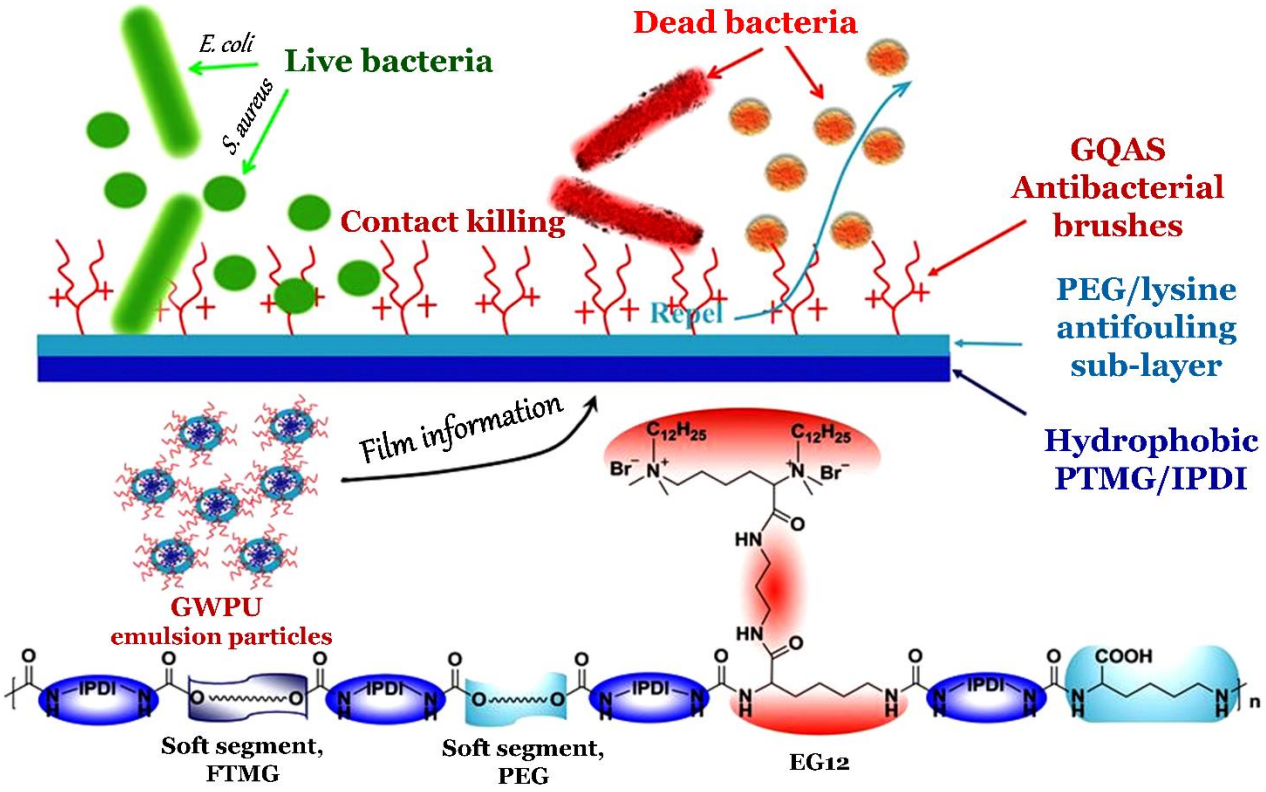

1371 **Figure 14.** The schematic of antibacterial and antifouling gemini quaternary ammonium salt

1372 polyurethane-based coating and the corresponding chemical structure. Reproduced with permission[150]

1373

1374

1375

1376

1377

1378

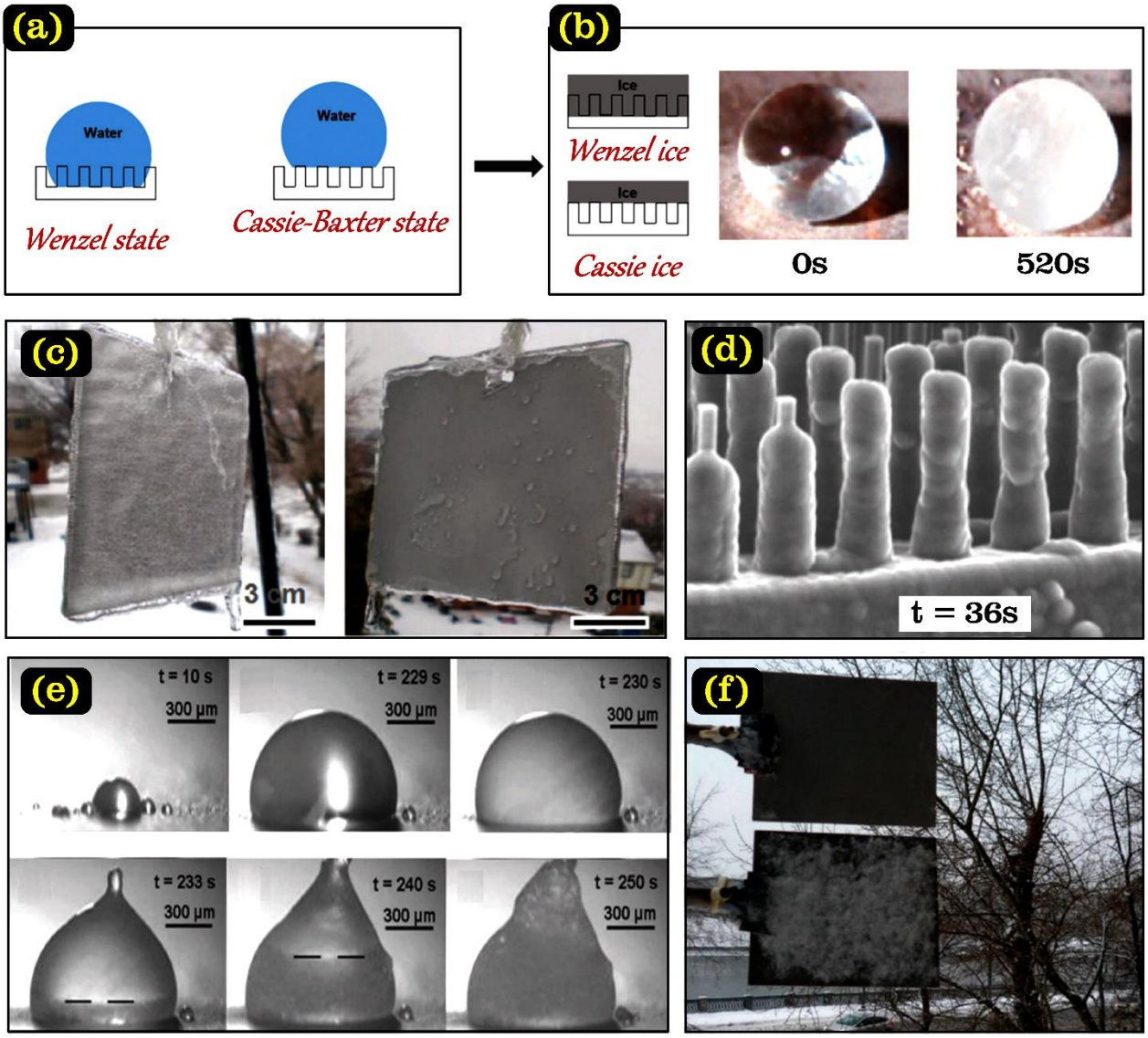

1379 **Figure 15.** Various anti-icing techniques for the preparation of ice-phobic coatings. Reproduced with

1380 permission[151]

1381

1382

1383

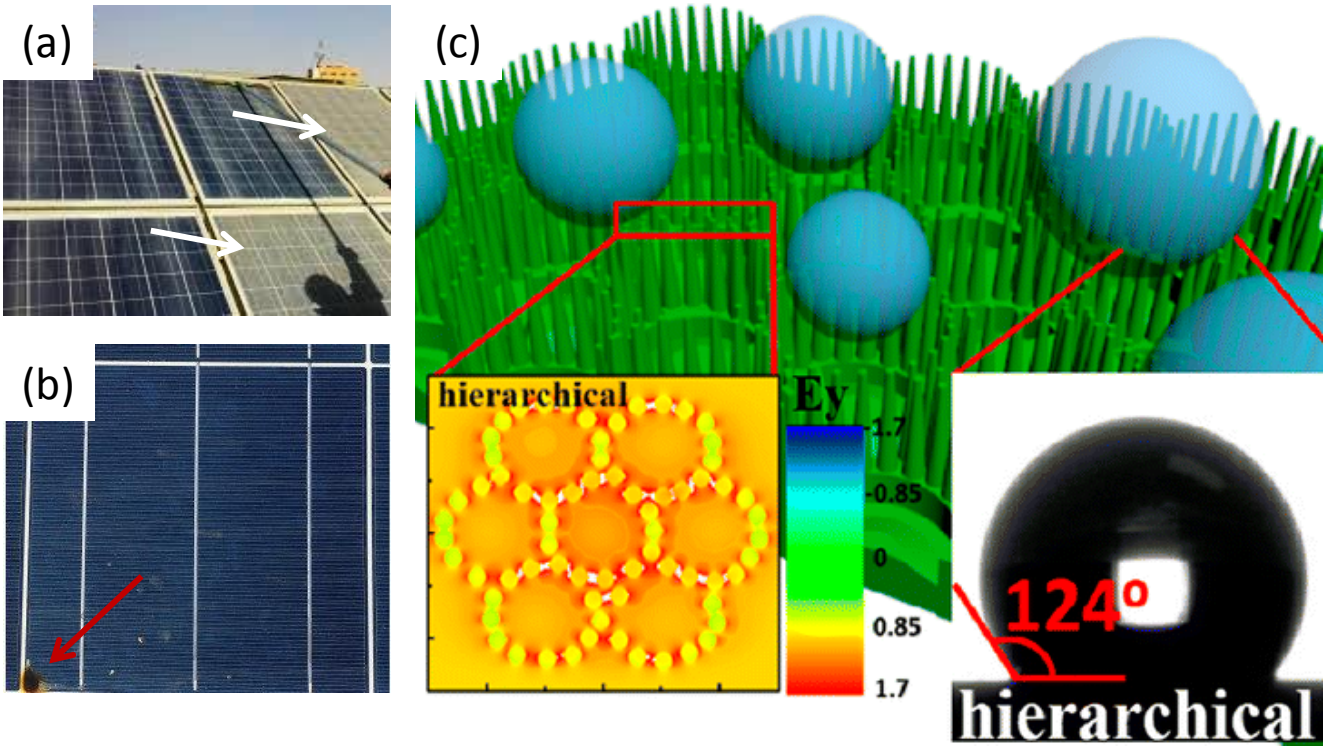

Figure 16. (a) examples of a dirty solar cell surface (while narrows); **(b)** a damaged panel (red narrow) due to formation of hot spots on a crystalline-silicon module; and **(c)** a self-cleaning omnidirectional solar cell. Reproduced with permission [235]